

# A NEW APPROACH TO SPHERICALLY SYMMETRIC JUNCTION SURFACES AND THE MATCHING OF FLRW REGIONS

U Kirchner

Department of Mathematics and Applied Mathematics

University of Cape Town

7700 Rondebosch, South Africa

e-mail: uli@maths.uct.ac.za

30. November 2003

## Abstract

We investigate timelike junctions between spherically symmetric solutions of the Einstein-field equation. In contrast to previous investigations this is done in a coordinate system in which the junction surface motion is absorbed in the metric, while all coordinates are continuous at the junction surface. Furthermore, there is no ambiguity in the direction of the normal vectors at the junction hypersurface.

We show that non-trivial timelike junction surfaces without surface layer (boundary surfaces) are generally not possible, except the metric components satisfy certain conditions.

We study the behaviour of the junction surface for small values of the surface energy density and show that in many cases the junction surface appears to reach the speed of light in a finite proper time. In other cases the junction surface approaches the speed of light asymptotically with respect to proper time on each side, but within a finite proper time measured along the junction.

For the junction between spherically symmetric space-time sections we show explicitly that the time component of the Lanczos equation always reduces to an identity.

We carefully discuss necessary and sufficient conditions for a possible matching of spherically symmetric space-time sections and apply the results to the matching of FLRW models.

Several junctions between FLRW models are studied numerically. Examples are given for junction surfaces which reach the speed of light within a finite and infinite time, respectively.

## 1 Introduction

Recent measurements of the microwave background radiation support the idea that our universe is highly isotropic and homogeneous [1]. Cosmological models with these properties are uniquely represented by the class of Friedmann-Lemaître-Robertson-Walker (FLRW) models. The observed flatness of the universe can then be explained by employing an inflationary model [2], which suggests an exponential expansion of the early universe driven by a scalar field – the inflaton field.

Nevertheless, it is often speculated that this might only be the local geometry, while over a larger scale the universe is inhomogeneous and anisotropic, i.e., the matter content and geometry vary. In particular, it appears as if the parameters necessary for life are highly fine-tuned and in order to solve this “fine-tuning problem” it was suggested that we live in one of many different FLRW regions – most of them might be unsuitable for life. The most prominent example is Linde’s Chaotic Inflation Scenario [3, 4], in which the different FLRW regions originate from different almost homogeneous Planck-sized regions which experience a period of exponential expansion.

When such models are discussed it is usually assumed that the transition region between two almost FLRW regions is very small and can be approximated by a timelike junction hypersurface, the so-called thin bubble wall. To find the motion of this hypersurface one has to find the matching surface to the two solutions of the Einstein-field equation representing the space-time on each side.

The matching conditions are of two different types. On the one hand there is the purely geometric necessity that ‘things fit together’ — distances on the junction surface should have the same length when measured ‘inside’ or ‘outside’. On a mathematical level this reduces to a matching of the tangential metric components.

On the other hand there are the matching conditions which result from the assumed validity of certain physical laws, in particular the energy-momentum conservation across the junction surface and the validity of the Einstein-field equation on each side. These conditions have been evaluated by C. Lanczos [5], R. Dautcourt [6], and in a ground-breaking work by W. Israel [7].

While these equations are in principle valid for any matching of two space-times satisfying the Einstein-field equation, it is in practice impossible to handle their complexity except for highly symmetric cases. In particular the matching of spherically symmetric space-times has been studied extensively (e.g., [7, 8, 9, 10]).

Our aim here is to present a new approach to junctions between spherically symmetric space-times and to apply the formalism to junctions between FLRW models — analytically and numerically.

The approach will focus on the geometrical quantities describing the situation, i.e., the distance of the junction surface from the centre of symmetry, and not alone on the junction surface radius. In contrast to most other studies, we do not evaluate the junction conditions (in particular the Lanczos equation) in the original coordinate system or in Gaussian normal coordinates based on the junction surface. Instead we introduce new coordinates such that the junction surface is at a fixed (new) ‘radial’ coordinate and all coordinates are continuous at the junction surface. The motion of the junction surface is now absorbed into the metric components and the continuity of the radial coordinate ensures the unambiguous identification of the normals on each side of the junction surface.

In spherically symmetric cases the Lanczos equation has two non-trivial independent components – an angular and a time component. While the first one leads to the well-known evolution equations, there seems to be uncertainty about the interpretation of the time component, which is a second order (in time) differential equation for the junction surface motion. It has been known that for certain particular cases this equation reduces to an identity [11]. Nevertheless, other authors<sup>1</sup> suggested that this equation acts as a surface equation of state [9], i.e., determines the surface pressure. Using the presented approach we will show that the time component of the Lanczos equation is in fact an identity for all junctions between spherically symmetric solutions of the Einstein-field equation.

It should be pointed out that there are special cases of junctions which could be examined without employing junction conditions. If the  $\gamma$ -equation of state and the cosmological constant have no discontinuity at the junction surface then the spherically symmetric space-time can be described in terms of the Lemaître-Tolman model. However, the really interesting question is how the junction behaves if the inside and outside region have different dynamical behaviour, i.e., different equation of state and cosmological constant. For these cases one cannot avoid the use of junction conditions and all numerical examples given in this Chapter will be of this kind.

This chapter will be structured as follows: In section 2 we re-examine junction conditions for the matching of generic spherically symmetric sections. We will re-derive the evolution and constraint equations using a new approach, based on a coordinate transformation which makes *all* coordinates continuous at the junction surface. We investigate the behaviour for small values of the surface-energy density and discuss the special case of vanishing surface-energy density. In section 3 we pay particular attention to constraints on the surface-energy density and in section 4 we show that the time-component of the Lanczos equation is an identity. This is followed by an application to the matching of FLRW sections in section 5 and numerous numerical examples in section 6.

## 1.1 Notations and Definitions

The Einstein summation convention will be used, i.e., any index which appears twice (once up and once down) in a term is understood to be summed over. We label the coordinates with greek indices, running from 0 to 3, where 0 represents the time coordinate. Latin indices label coordinates on the three-dimensional junction surface hypersurface. As will be seen below, with our choice of coordinates the junction surface is located at a fixed radial coordinate  $R = 1$ , and hence latin indices take the values 0, 2, and 3 (or equivalently  $t$ ,  $\theta$ , and  $\phi$ ).

We will use the convention that round/square brackets around indices represent the symmetrization/anti-symmetrization operator, i.e.,  $T_{(\mu\nu)} \stackrel{\text{def}}{=} \frac{1}{2}(T_{\mu\nu} + T_{\nu\mu})$  and  $T_{[\mu\nu]} \stackrel{\text{def}}{=} \frac{1}{2}(T_{\mu\nu} - T_{\nu\mu})$ .

We use a metric signature  $(-+++)$ , i.e.,  $u_\mu u^\mu < 0$  if and only if  $u_\mu$  is a timelike vector. The Christoffel symbols are given in terms of the metric by

$$\Gamma_{\mu\nu\lambda} \stackrel{\text{def}}{=} \frac{1}{2}(g_{\mu\nu,\lambda} + g_{\lambda\mu,\nu} - g_{\nu\lambda,\mu}),$$

---

<sup>1</sup>In particular this was suggested for the junction between FLRW models.

where a comma indicates the ordinary partial derivative with respect to the coordinates, e.g.,  $g_{\mu\nu,\lambda} = \frac{\partial}{\partial x^\lambda} g_{\mu\nu}$ . The covariant derivative of a vector  $u^\mu$  is then given by

$$u^\mu{}_{;\nu} = u^\mu{}_{,\nu} + u^\lambda \Gamma^\mu{}_{\nu\lambda} \quad u_{\mu;\nu} = u_{\mu,\nu} - u_\lambda \Gamma^\lambda{}_{\nu\mu}.$$

When considering quantities defined for certain hypersurfaces (like the junction surface) it will be convenient to have a covariant derivative for this subspace. We will use a vertical bar (like in  $K_{ab|c}$ ) to refer to this covariant hypersurface derivative, which is evaluated in the same way as above covariant derivative, but with all quantities replaced by the corresponding hypersurface quantities. Any quantity referring to the three-dimensional hypersurface of the junction surface will have a superscript ‘(3)’, e.g.,  ${}^{(3)}R$  and  ${}^{(3)}g_{ab}$ .

The Riemann curvature tensor is defined in terms of the Christoffel symbols by

$$R^\nu{}_{\lambda\kappa}{}^\mu{}_{\lambda\kappa} \stackrel{\text{def}}{=} \Gamma^\nu{}_{\lambda\mu,\kappa} - \Gamma^\nu{}_{\kappa\mu,\lambda} + \Gamma^\alpha{}_{\lambda\mu} \Gamma^\nu{}_{\kappa\alpha} - \Gamma^\alpha{}_{\kappa\mu} \Gamma^\nu{}_{\lambda\alpha}.$$

The Ricci tensor and scalar are defined as contractions of the Riemann curvature tensor by  $R_{\mu\nu} \stackrel{\text{def}}{=} R^\lambda{}_{\mu\lambda\nu}$  and  $R \stackrel{\text{def}}{=} R^\mu{}_\mu$ .

We will use a subscript  $-$  or  $+$  sign to indicate whether quantities refer to the in- or outside region, respectively.

## 2 Matching of generic O(3)-symmetric sections

### 2.1 The coordinate system

Any spherically symmetric space-time (i.e., having O(3) symmetry) allows coordinates such that the metric takes the form

$$ds^2 = -\mathfrak{N}^2(\tau, r) d\tau^2 + l^2(\tau, r) \{dr^2 + f^2(\tau, r) d\Omega^2\}, \quad (1)$$

where  $\mathfrak{N}(\tau, r)$  is the so-called lapse function, and  $d\Omega^2 = d\theta^2 + \sin^2(\theta) d\phi^2$  the line-element on the two-dimensional unit-sphere.

We are interested in the matching of two spherically symmetric space-times, each having a metric of the form (1). Generally, the coordinates will not match up at the junction surface and the manifold is described by two different coordinate charts – one for the inside region (subscript  $-$ ) and one for the outside region (subscript  $+$ ). At any coordinate time (in the inside or outside region) the junction surface itself is assumed to be a two-sphere which is described by its coordinate radius in the inside and outside region,  $\alpha_-(\tau_-)$  and  $\alpha_+(\tau_+)$ .

Since the inside and outside regions are originally described by a metric in the form (1) we will use the convention that a dot/prime refers to the proper time/radial derivative with respect to the metric (1) at the junction surface, e.g.,

$$\dot{l}_+ \stackrel{\text{def}}{=} \frac{1}{\mathfrak{N}_+} \frac{\partial}{\partial \tau} l_+(\tau, r) \Big|_{r=\alpha_+(\tau_+)} \quad \text{and} \quad l'_+ \stackrel{\text{def}}{=} \frac{1}{l_+} \frac{\partial}{\partial r} l_+(\tau, r) \Big|_{r=\alpha_+(\tau_+)}.$$

While the angular coordinates  $\theta$  and  $\phi$  can be chosen such that they are continuous at the junction surface, this is generally not true for the radial and time coordinates  $r$  and  $t$  – the same point on the junction surface is represented by different coordinate values on each side. In order to describe the motion of the junction surface one usually tries to find the evolution of the junction surface radius in each coordinate system.

We want to suggest a different approach: we introduce a new coordinate system, such that *all* the coordinates are continuous at the junction surface while only the transverse metric components are discontinuous at the junction surface. The junction surface motion is now described by the evolution of the metric components.

**Constructing a continuous time coordinate** Let us assume that the inside and outside spaces are given in terms of their metrics, which take the form (1). Generally the time coordinates for the inside and outside region will not match up at the junction hypersurface. Nevertheless, it is possible to re-scale the time coordinate on each side of the junction surface by setting

$$d\tau = \eta(t) dt$$

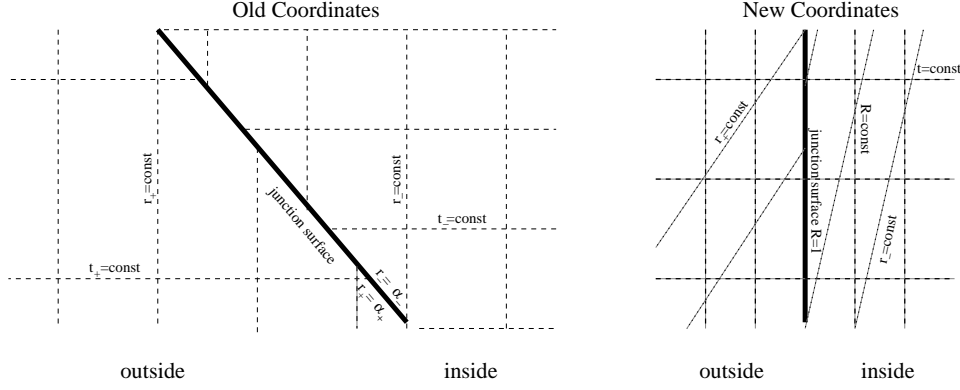


Figure 1: An illustration of the coordinate transformation. The original radial coordinates  $r_+$  and  $r_-$  are rescaled such that in the new coordinate system the junction surface is at a fixed ‘radial’ coordinate  $R = 1$ . The time-coordinates are rescaled such that they match up at the junction surface.

in such a way that the new time coordinates  $t_+$  and  $t_-$  match up at the junction surface. This gives us a ‘global time coordinate’  $t$ .

If the original lapse function was constant then this re-scaling results in a new time dependent lapse function which contains information about the junction surface motion. For example, this will be the case for the matching of FLRW models.

If on the other hand the original lapse function  $\mathfrak{N}(\tau, r)$ , where  $\tau$  is the original time coordinate, depends on the radial coordinate then we can write the new lapse function (which makes the time coordinate continuous) as

$$N(t, r) = \eta(t) \mathfrak{N}(\tau, r),$$

where  $\tau = \int_0^t \eta(t') dt'$  and  $t$  is the new time coordinate. It is now  $\eta(t)$  which contains information about the junction surface motion, while  $\mathfrak{N}$  contains information about the background space. In particular the quantity

$$\frac{N'(t, r)}{N(t, r)} = \frac{\mathfrak{N}'(\tau, r)}{\mathfrak{N}(\tau, r)}$$

(taken as a function of proper time) does not depend on  $\eta$ . We will keep these issues in mind when we use the lapse function in the following calculations.

**Constructing a continuous radial coordinate** Now we want to construct new radial coordinates such that the junction surface is at a fixed radial coordinate  $R = 1$ . This can be achieved by setting  $r_{\pm} = \alpha_{\pm}(t)R$ , where the subscript  $+$  refers to outside ( $R > 1$ ) and  $-$  to the inside region, and  $\alpha_{\pm}(t)$  is the coordinate radius of the junction surface at time  $t$ . The relation between the old and the new coordinates is illustrated in figure 1. With this new radial coordinate the metrics for the inside and outside region take the form

$$ds^2 = -N^2 \{1 - R^2 \dot{\alpha}^2 l^2\} dt^2 + 2\alpha N \dot{\alpha} l^2 R dR dt + l^2 \{\alpha^2 dR^2 + f^2(\alpha R) d\Omega^2\}, \quad (2)$$

where a dot indicates the proper time derivative along paths of constant  $r, \theta, \phi$ , i.e.,  $\dot{\alpha} \stackrel{\text{def}}{=} \frac{1}{N} \frac{\partial}{\partial t} \alpha$ . It will be useful to have the inverse metric at hand, which takes the form

$$g^{\mu\nu} = \begin{pmatrix} -\frac{1}{N^2} & \frac{\dot{\alpha} R}{\alpha N} & 0 & 0 \\ \frac{\dot{\alpha} R}{\alpha N} & \frac{1 - R^2 \dot{\alpha}^2 l^2}{l^2 \alpha^2} & 0 & 0 \\ 0 & 0 & \frac{1}{l^2 f^2} & 0 \\ 0 & 0 & 0 & \frac{1}{l^2 f^2 \sin^2(\theta)} \end{pmatrix}. \quad (3)$$

## 2.2 Geometric matching conditions

At the matching surface  $R = 1$  the tangential metric components must be continuous. This gives us the two matching conditions

$$[lf] = 0. \quad (4)$$

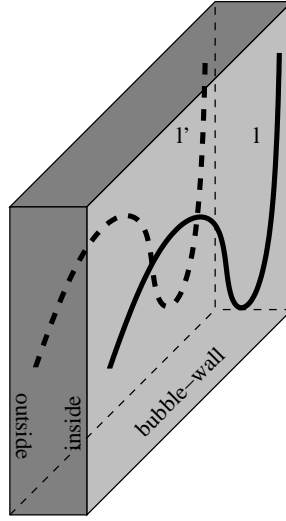


Figure 2: The geometric matching condition ensures that curves on the hypersurface measure the same length on each side of the junction surface.

and

$$[N^2(\dot{\alpha}^2 l^2 - 1)] = 0, \quad (5)$$

where

$$[g(R)] \stackrel{\text{def}}{=} \lim_{R \rightarrow 1^+} (g(R)) - \lim_{R \rightarrow 1^-} (g(R)) = \lim_{r \rightarrow \alpha(t)^+} (g(r)) - \lim_{r \rightarrow \alpha(t)^-} (g(r)).$$

These relations identify two quantities which are continuous across the junction surface and we define

$$k(t, R) \stackrel{\text{def}}{=} N \sqrt{1 - \dot{\alpha}^2 l^2 R^2} \quad , \quad k \stackrel{\text{def}}{=} k(t, 1) = N \sqrt{1 - \dot{\alpha}^2 l^2} \Big|_{R=1} \quad (6)$$

and

$$w \stackrel{\text{def}}{=} l f, \quad (7)$$

which are the tangential metric components. Note that  $k(t, R)$  becomes complex for large  $\dot{\alpha}^2 l^2 R^2$ . However, this is not of relevance for the problem at hand, since we are only interested in the behaviour around the junction surface at  $R = 1$  where  $k(t, R)$  is real for timelike junction surfaces.

It follows from (5) that if the surface appears from one side as timelike, it will so from the other side. From now on let us assume that the junction surface is a timelike surface, *i.e.*,  $\dot{\alpha}_{\pm} l_{\pm} < 1$ .

There is a remaining gauge freedom: we can rescale the global time coordinate, *i.e.*, multiply the lapse functions with a time dependent factor. One particularly useful choice is to rescale the time such that the tangential metric component in the timelike direction parallel to the junction surface becomes unity, *i.e.*,

$$k = N \sqrt{1 - \dot{\alpha}^2 l^2} \Big|_{R=1} = 1. \quad (8)$$

To maintain generality we will not assume this choice until explicitly stated (in section 2.4).

The two conditions (4) and (5) are of pure geometric character – they have to be satisfied independently of the evolution equations at all times. Taking the total derivative of (7) with respect to coordinate time we obtain the corresponding restriction on the junction surface motion

$$\frac{dw}{dt} = N \{ (lf)^{\bullet} + (lf)' \dot{\alpha} l \} \quad \left[ \frac{dw}{dt} \right] = 0. \quad (9)$$

It should be noted that here  $N$  is not independent, but depends via (8) on the junction surface motion. Equations (8) and (9) generally have two solutions for the junction surface motion in terms of the surface radius evolution.

Let us note here that the metric of the timelike hypersurface representing the junction surface is given by

$$^{(3)}g_{\mu\nu} dx^{\mu} dx^{\nu} \stackrel{\text{def}}{=} ds_{\Sigma}^2 = -k^2 dt^2 + w^2 d\Omega^2.$$

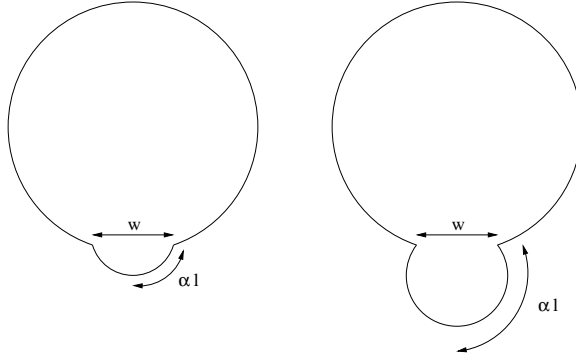


Figure 3: The junction surface radius  $w$  does not necessarily identify the position of the junction surface, represented by  $\alpha l$ . Here the two matching ‘surfaces’ have the same surface radius  $w/2$ , but different positions  $\alpha l$ .

The intrinsic geometry of the junction hypersurface is completely defined by  $k$  and  $w$ . Nevertheless,  $w$  might not uniquely identify the position of the junction surface as is illustrated in figure 3. Only if  $l_+ f_+$  and  $l_- f_-$  are invertible functions of  $\alpha_{\pm}$  then the position of the junction surface is indirectly given by the value of  $w$ . It can easily be seen that the derivatives of  $lf$  are given by

$$-(lf) \frac{\partial(lf)}{\partial x^\mu} = \Gamma_{\mu\theta\theta},$$

and in particular the evolution of the junction surface radius with respect to coordinate time is

$$\frac{\partial w}{\partial t} = -\frac{1}{w} \Gamma_{t\theta\theta},$$

which is continuous across the junction surface.

### 2.3 Lanczos equation and Israel junction conditions

Let us split the energy-momentum tensor in a regular and a  $\delta$ -function part, so that

$$T_{\mu\nu} = \delta(\eta) S_{\mu\nu} + \tilde{T}_{\mu\nu}, \quad (10)$$

where  $\tilde{T}_{\mu\nu}$  contains the regular part and  $\eta$  is a function of the coordinates which vanishes on the junction surface, is non-zero everywhere else, and on the junction surface its gradient is a unit vector. The tensor  $S_{\mu\nu}$  is called the surface stress-energy (or energy-momentum) tensor. The  $\delta$ -function restricts its influence to the junction surface and we assume that it only depends on coordinates on the junction surface, i.e., in our case this tensor does not depend on  $R$ . The Lanczos equation [5] relates the surface energy-momentum tensor  $S_{\mu\nu}$  to the jump in the extrinsic curvature  $K_{\mu\nu}$  of the junction surface by

$$\kappa S^{\mu\nu} = {}^{(3)}g^{\mu\nu} [K] - [K^{\mu\nu}], \quad (11)$$

or equivalently (after taking the trace and substituting back for  $K$ )

$$\frac{1}{\kappa} [K^{\mu\nu}] = -S^{\mu\nu} + \frac{1}{2} {}^{(3)}g^{\mu\nu} S, \quad (12)$$

where  $K \stackrel{\text{def}}{=} K^\mu{}_\mu$ ,  $S \stackrel{\text{def}}{=} S^\mu{}_\mu$ , and  $\kappa \stackrel{\text{def}}{=} 8\pi G$ . These two equations imply that the presence of a surface layer is equivalent to a jump in the extrinsic curvature, i.e.,  $\gamma^{\mu\nu} \stackrel{\text{def}}{=} [K^{\mu\nu}] \neq 0$ .

To relate this conditions to the metric components on both sides of the junction surface we have to find expressions for the extrinsic curvature. We start with the normal to the junction surface, which is given by

$$n_\mu = \delta_\mu^R \frac{l\alpha}{\sqrt{1 - R^2 \dot{\alpha}^2 l^2}} \Big|_{R=1}, \quad (13)$$

and the unique timelike unit-vector tangential to the junction surface and orthogonal to the spherical symmetric subspace, which is given by

$$u^\mu = \frac{1}{k} \delta_t^\mu. \quad (14)$$

The projection tensor for the junction surface becomes

$$h^{\mu\nu} = g^{\mu\nu} - n^\mu n^\nu = u^\mu u^\nu + \frac{1}{l^2 f^2} (\delta_\theta^\mu \delta_\theta^\nu + \sin^{-2}(\theta) \delta_\phi^\mu \delta_\phi^\nu)$$

and the extrinsic curvature on each side of the junction surface is given by

$$K_{\mu\nu} = \frac{1}{2} (h_{\mu\nu;\lambda} n^\lambda + n_{\mu;\nu} + n_{\nu;\mu}) = n_{(\lambda;\kappa)} h^\lambda_\mu h^\kappa_{\nu}. \quad (15)$$

It is easy to verify that the extrinsic curvature is symmetric and tangential, i.e.,  $K_{\mu\nu} = K_{(\mu\nu)}$  and  $K_{\mu\nu} n^\mu = 0$ . From (15) we derive convenient expressions for the extrinsic curvature of the junction surface in terms of unit-vector derivatives and Christoffel-symbols. In particular, the two independent components are given by

$$K_{\mu\nu} u^\mu u^\nu = -n_\mu u^\mu{}_{;\nu} u^\nu = \frac{l\alpha N}{k^3} \Gamma^R_{tt} \quad (16)$$

$$K_{\theta\theta} = n_\rho \Gamma^\rho_{\theta\theta} = \frac{Nlf}{k} \Gamma^R_{\theta\theta}. \quad (17)$$

Setting  $k = 1$  (for all times) and using the coordinate time derivative of (8) we find

$$K_{\mu\nu} u^\mu u^\nu = \frac{1}{Nl\alpha} \Gamma_{Rtt} = -\frac{\dot{N} + 2N'l\dot{\alpha} + \dot{\alpha}^2 l^2 N(i/l)}{\dot{\alpha}l}. \quad (18)$$

$$K^\theta_\theta = \frac{N}{w} (\dot{\alpha}l(fl)^\bullet + (lf)'). \quad (19)$$

This form of the extrinsic curvature implies that the surface energy-momentum tensor  $S^{\mu\nu}$  is diagonal and of perfect-fluid form (in the three-dimensional hypersurface space). We introduce the surface energy density  $\rho_s$  and pressure  $p_s$  such that

$$S^{\mu\nu} = (\rho_s + p_s) u^\mu u^\nu + p_s {}^{(3)}g^{\mu\nu}. \quad (20)$$

The Lanczos equations (12) are now given by the two independent equations

$$[N\{\dot{\alpha}l(fl)^\bullet + (lf)'\}] = -\frac{\kappa}{2} \rho_s w k \quad (21)$$

$$\left[ \dot{N} + 2N'l\dot{\alpha} + \dot{\alpha}^2 l^2 N(i/l) \right] = \kappa \left( \frac{1}{2} \rho_s + p_s \right) k^3. \quad (22)$$

The Gauss-Codazzi equations relate the curvature at one point to the extrinsic and intrinsic curvature of a hypersurface which passes through this point. Let us first define coordinate basis vectors tangential to the junction surface by

$$e_a{}^\mu \stackrel{\text{def}}{=} \frac{\partial x^\mu}{\partial \xi^a},$$

where  $\xi^a$  are the coordinates covering the junction surface (in our case  $t, \theta, \phi$ ). The Gauss-Codazzi equations are then given by

$$R_{\mu\nu\lambda\kappa} e_a{}^\mu e_b{}^\nu e_c{}^\lambda e_d{}^\kappa = {}^{(3)}R_{abcd} + \epsilon (K_{ad} K_{bc} - K_{ac} K_{bd})$$

and

$$R_{\mu\nu\lambda\kappa} n^\mu e_b{}^\nu e_c{}^\lambda e_d{}^\kappa = K_{bc|d} - K_{bd|c},$$

where a vertical bar denotes the covariant derivative with respect to the induced hypersurface metric  $h_{\mu\nu} = g_{\mu\nu} - n_\mu n_\nu$ , and  $\epsilon \stackrel{\text{def}}{=} n^\mu n_\mu$  equals  $+1$  for timelike hypersurfaces, and  $-1$  for spacelike hypersurfaces. For a timelike hypersurface these equations lead to [12]

$$2G_{\mu\nu} n^\mu n^\nu = -{}^{(3)}R + K^2 - K_{\mu\nu} K^{\mu\nu} \quad (23)$$

$$G_{\mu\nu} e_a{}^\mu n^\nu = K_a{}^b{}_{|b} - K_{|a}, \quad (24)$$

where  $G_{\mu\nu} \stackrel{\text{def}}{=} R_{\mu\nu} - \frac{1}{2}g_{\mu\nu}R$  is the Einstein tensor. Substituting (12) into (23) and (24) gives

$$[G_{\mu\nu}e_a^\mu n^\nu] = -\kappa S_a^b|_b \quad (25)$$

$$[G_{\mu\nu}n^\mu n^\nu] = \frac{1}{2}[K^2 - K_{\mu\nu}K^{\mu\nu}] = \kappa S^{\mu\nu}\bar{K}_{\mu\nu}, \quad (26)$$

where  $\bar{K}_{\mu\nu} \stackrel{\text{def}}{=} \frac{1}{2}(\lim_{R \rightarrow 1^+} K_{\mu\nu} + \lim_{R \rightarrow 1^-} K_{\mu\nu})$ . The second of these equations represents nothing else than the definition of the surface stress-energy tensor  $S^{\mu\nu}$  (which was substituted) and hence is redundant. Using (20) to evaluate (25) we find that the only non-vanishing component is the time component, which is given by (using  $e_0^\mu = u^\mu$ )

$$ku^\mu \rho_{s;\mu} + k(\rho_s + p_s)u^a|_a = \kappa^{-1}[G_{\mu\nu}u^\mu n^\nu] = [T_{\mu\nu}u^\mu n^\nu], \quad (27)$$

where the last equality follows from the Einstein equation and  $u^a|_a = u^\mu(2\ln(lf))_{;\mu}$ . Together with an equation of state for the surface energy and pressure densities this equation describes the evolution of the ‘matter’ on the surface.

On the other hand (26) becomes after substituting (20) and (16)

$$-(\rho_s + p_s)\overline{n_\mu u^\mu}_{;\nu} u^\nu + p_s \bar{K} = \kappa^{-1}[G_{\mu\nu}n^\mu n^\nu] = [T_{\mu\nu}n^\mu n^\nu - \Lambda/\kappa].$$

## 2.4 Matching with surface-layer

The second geometric matching condition shows that  $k \stackrel{\text{def}}{=} N\sqrt{1 - \dot{\alpha}^2 l^2}$  is continuous across the junction surface. Hence we can express the junction surface motion in terms of the lapse function by

$$\dot{\alpha}l = \pm \sqrt{1 - \left(\frac{k}{N}\right)^2}. \quad (28)$$

For convenience we will choose now  $k = 1$ , i.e., the coordinate time corresponds to proper time along the curves  $R = 1, \theta, \phi$  constant on the junction surface. Setting  $u \stackrel{\text{def}}{=} N/k$  and  $j_\pm \stackrel{\text{def}}{=} \text{sign}(\dot{\alpha}_\pm)$  the angular component of the extrinsic curvature (19) on both sides of the junction surface and equation (9), the derivative of the junction surface radius with respect to coordinate time, are given by

$$K^\theta_\theta = (uw' + j\dot{w}\sqrt{u^2 - 1})/w \quad (29)$$

$$L \stackrel{\text{def}}{=} \frac{dw}{dt} = u\dot{w} + jw'\sqrt{u^2 - 1} \quad (30)$$

A valid matching between two spherically symmetric sections, each satisfying the Einstein-field equations, must satisfy the two geometric matching conditions ((4) and (5)) and the two independent components of the Lanczos equation ((21) and (22)). We first note, that if the first geometric matching condition (matching of the surface radius) (4) is satisfied initially, then it is sufficient to demand that its coordinate time derivative (9) is satisfied at all times. Secondly, with our choice of variables the second geometric matching condition (5) is nothing more than an identity — with (28) it has already been used to eliminate one variable. Thirdly, as will be shown in section 4, equation (22), the time-component of the Lanczos equation, is in fact identically satisfied if all the other matching conditions are satisfied, the Einstein-field equations are valid on each side, and the surface-matter evolution is given by (27).

We conclude that the matching conditions are completely represented by (9), the coordinate time derivative of the first geometric matching condition, and the angular component of the Lanczos equation (21) together with an initial matching of the proper surface radius  $w = lf$ . With our choice of variables these equations take the (surprisingly symmetric) form

$$[L] = [u\dot{w} + jw'\sqrt{u^2 - 1}] = 0 \quad (31)$$

$$[wK^\theta_\theta] = [uw' + j\dot{w}\sqrt{u^2 - 1}] = -E, \quad (32)$$

where  $w \stackrel{\text{def}}{=} lf$  is the proper surface radius of the spherical junction surface on each side and

$$E \stackrel{\text{def}}{=} \frac{\kappa \rho_s w}{2} \quad (33)$$



quantifies the energy-content of the layer. To find a relation between  $K^\theta_\theta$  and  $L$  we square (29) and substitute  $L^2$  from the square of (30) and obtain

$$(wK^\theta_\theta)^2 = L^2 + a, \quad (34)$$

where  $a \stackrel{\text{def}}{=} w'^2 - \dot{w}^2$ . Versions of this equation have been given in [9] and [13]. For  $E \neq 0$  we can express  $K^\theta_\theta$  in terms of  $L$  by using an algebraic identity as

$$wK^\theta_\theta = \frac{[(wK^\theta_\theta)^2] \pm [wK^\theta_\theta]^2}{2[wK^\theta_\theta]} = \frac{b \pm E^2}{-2E}, \quad (35)$$

where  $b \stackrel{\text{def}}{=} a_+ - a_-$ . The explicit expression for  $L$  in terms of  $E$  takes the form

$$L^2 = \left( \frac{b - E^2}{2E} \right)^2 - a_- = \left( \frac{b + E^2}{2E} \right)^2 - a_+ = (E^4 - 2E^2(a_+ + a_-) + b^2)/4E^2, \quad (36)$$

Note that we find by differentiating (29) and (30) with respect to  $u$  (taking  $w$ ,  $\dot{w}$ , and  $w'$  to be independent of  $u$ ) the helpful relations

$$j\sqrt{u^2 - 1} \frac{\partial L}{\partial u} = wK^\theta_\theta \quad \text{and} \quad j\sqrt{u^2 - 1} \frac{\partial wK^\theta_\theta}{\partial u} = L, \quad (37)$$

which are valid on each side of the junction surface.

The geometric matching condition (30) can be solved for  $u_\pm$  and  $j_\pm$  in terms of the time derivative of the surface radius  $L$  and the extrinsic curvature component  $K^\theta_\theta$

$$u = \frac{\dot{w}L - w'wK^\theta_\theta}{-a}. \quad (38)$$

We note that differentiating (38) with respect to  $u$  and using (37) yields

$$j\sqrt{u^2 - 1} = \frac{w'L - \dot{w}wK^\theta_\theta}{a}, \quad (39)$$

what also determines the sign of  $j$  and hence the radial direction of motion of the junction surface for each side.

## 2.5 The ‘no surface-layer’ case

If all tangential components of the extrinsic curvature are continuous at the junction surface then it follows from (32) that the surface-energy density  $\rho_s$  vanishes. In this case the junction hypersurface is called a boundary-surface.

It is an immediate consequence of (34) that in this case

$$b = [a] = [w'^2 - \dot{w}^2] = 0.$$

Feasible solutions need to satisfy the two geometric matching conditions (4) and (5), the derivative of the first matching condition (9) and the matching of the extrinsic curvature (21). Recognizing the similar structure of (9) and (21) we form two new equivalent equations by adding and subtracting the two equations. The result reads

$$[N(1 - \dot{\alpha}l)(w' - \dot{w})] = 0 \quad [N(1 + \dot{\alpha}l)(w' + \dot{w})] = 0.$$

Using the factorized form of the second geometric matching condition (5) and defining  $q = N(1 - \dot{\alpha}l)$  this becomes

$$[q(w' - \dot{w})] = 0 \quad \left[\frac{1}{q}(w' + \dot{w})\right] = 0.$$

If both  $w' - \dot{w}$  and  $w' + \dot{w}$  vanish separately on both sides, then the system becomes an identity and the junction surface motion remains undefined. Let us assume now that this is not the case.

We note that for  $[w'] = [\dot{w}] = 0$  the system is solved for any  $q_+ = q_-$ . If the angular component of the metric and its first order proper time and radial derivatives are continuous, then the junction surface motion does not follow from the matching conditions. In particular, this is the case for the trivial matching of two identical space-times, where we have an ‘imaginary junction surface’, which could be placed anywhere.

Let us from now on assume that at least one of the proper derivatives of  $w$  is not continuous at the junction surface. It is easy to see from above system that there are no solutions to the system if  $w' \pm \dot{w} \neq 0$  on both sides.

If  $w' \pm \dot{w}$  is zero on one side, it has to be zero on the other side too (otherwise no matching is possible) and the solutions have to satisfy

$$\frac{N_- \sqrt{1 - \dot{\alpha}_-^2 l_-^2}}{N_+ \sqrt{1 - \dot{\alpha}_+^2 l_+^2}} = \frac{w'_\pm}{w'_\mp}.$$

We conclude that a matching without surface-layer is only possible for some exceptional situations. The junction-motion is only defined if either  $w' + \dot{w} = 0$  or  $w' - \dot{w} = 0$  (but not both) on each sides. If  $w'$  and  $\dot{w}$  are continuous at the junction surface then the motion remains undefined – ‘there is no real junction’.

## 2.6 Expansion for small surface-energy densities

As will be seen in the numerical examples given later, in many cases the surface-energy density (and hence  $E$ ) approaches zero at some finite coordinate time. In this case the dynamic quantities can be approximated by a series expansion in terms of  $E$ . We start by re-writing the exact expression for the extrinsic curvature (35) as

$$wK_{\pm\theta}^\theta = -\frac{b}{2E} \mp \frac{E}{2}.$$

It follows then from (36) that

$$\pm L = \frac{|b|}{2E} - \frac{a_+ + a_-}{2|b|}E + O(E^3),$$

where  $O(E^3)$  represents terms of the order  $E^3$  or smaller. Furthermore, from (38) we find for  $u = N/k$  the expansion

$$u_\pm = -\frac{w'_\pm b + \text{sign}(L)\dot{w}_\pm |b|}{2a_\pm} \frac{1}{E} + \frac{\text{sign}(L)\dot{w}_\pm (a_+ + a_-)/|b| \mp w'_\pm}{2a_\pm} E + O(E^3).$$

As the surface-energy density approaches zero the lapse functions (given by  $u_+$  and  $u_-$ ) diverge and the proper speed of the junction surface approaches the speed of light quadratically since

$$|\dot{\alpha}_\pm l_\pm| = 1 - \frac{2\alpha_\pm l_\pm^2}{w'_\pm b + \text{sign}(L)\dot{w}_\pm |b|} E^2 + O(E^4).$$

To examine if and how  $E$  approaches zero we finally expand the evolution equation (27)

$$\frac{dE}{dt} = \frac{\kappa}{2} \left( w[T_{\mu\nu} u^\mu n^\nu] - \frac{|b|}{w} \left( \gamma_s - \frac{1}{2} \right) \right) + O(E^2).$$

Generally the first term diverges as we approach the speed of light — for example in the case of a perfect fluid one finds

$$|T_{\mu\nu} u^\mu n^\nu| = \left( \frac{w'b + \text{sign}(L)\dot{w}|b|}{2a} \right)^2 (\rho + p) \frac{1}{E^2} + O(E^0).$$

We conclude that if the energy-momentum contribution  $[T_{\mu\nu} u^\mu n^\nu]$  has a sign opposite to  $E$ , then  $E$  accelerates towards zero. In many cases  $E$  will reach zero at some finite coordinate time  $t_0$ . Close to this point and assuming that the time dependence of all other terms is negligible we have  $E \propto (t_0 - t)^{1/3}$ . This implies that the lapse functions are integrable and the junction surface reaches the speed of light (on each side) within a finite proper time. Here our formalism breaks down and one would need a separate treatment of these singular cases. We want to speculate here that at these points the junction surface turns spacelike.

On the other hand, if the sign of  $[T_{\mu\nu} u^\mu n^\nu]$  is the same as the sign of  $E$  then  $E$  cannot get arbitrarily close to zero. In some cases (see figure 11)  $E$  will oscillate around some value (which is itself time dependent). Even in these cases we can encounter divergencies resulting from diverging  $a_\pm$  and  $b$ . This can lead to non-integrable lapse functions - from each side the junction seems to exist forever, but an observer who moves along the junction encounters a singular point after a finite time. At this point the surface energy density is zero and again the formalism breaks down.

It should be noted that in the case of a perfect fluid on both sides of the junction the sign of the stress-energy contribution  $[T_{\mu\nu} u^\mu n^\nu]$  depends on the energy density  $\rho$  and pressure  $p$  on both sides, i.e., on the

equations of state. Hence whether a particular junction reaches the speed of light within a finite time or not might depend on the equation of state on each side. In section 6 we give a numerical example for such a case.

Because points on the junction surface are not causally connected a spacelike junction surface has a very different physical interpretation. In such cases the junction surface cannot be treated as an ‘evolving system’ on its own, but rather as some kind of (spacelike) transition surface which is generated by the physics underlying the cosmological model.

Usually a timelike junction surface is used to model the time evolution of a spatially *localized* inhomogeneity. If a junction surface turns spacelike a breakdown in the thin wall approximation must have occurred.

### 3 Necessary and sufficient conditions for a possible matching

#### 3.1 Demanding real solutions for $L$

From (36) we find with  $L^2 \geq 0$  a necessary condition for the existence of solutions which restricts the allowed values for  $E$ , such that

$$E^4 - 2E^2(a_+ + a_-) + b^2 \geq 0. \quad (40)$$

The roots of the quadratic polynomial (in  $E^2$ ) on the left-hand side are given by  $a_+ + a_- \pm 2\sqrt{a_+a_-}$ . For  $a_+a_- < 0$  the quadratic has no root and all values of  $E$  are feasible. If on the other hand, both  $a_+$  and  $a_-$  are negative then (40) has only negative roots for  $E^2$  and hence all real values of  $E$  are feasible. For  $a_+, a_- \geq 0$  the roots become  $|\sqrt{a_+} \pm \sqrt{a_-}|$  and the feasible values for  $E$  are

$$0 \leq |E| \leq |\sqrt{a_+} - \sqrt{a_-}| \quad \text{or} \quad \sqrt{a_+} + \sqrt{a_-} \leq |E|. \quad (41)$$

The shape of the forbidden region in the  $E - a_+ - a_-$  and  $E - \sqrt{a_+}$  space is illustrated in figures 4 and 5, respectively.

**Figure omitted in the arXiv version.**

**Figure 4: The shaded volume represents the region in the  $E - a_+ - a_-$ -space where there is no solution for the junction surface motion.**

For  $a_+, a_- \geq 0$  it is easily verified that

$$0 \leq |\sqrt{a_+} - \sqrt{a_-}| \leq \sqrt{|a_+ - a_-|} \leq \sqrt{a_+} + \sqrt{a_-}$$

and hence the two disjoint regions allowed for  $E$  given by (41) are easily distinguished by  $E^2 \leq |b|$  and  $E^2 \geq |b|$ . Furthermore, from (35) we find  $\text{sign}(K_{-\theta}^\theta) = \text{sign}(K_{+\theta}^\theta) = -\text{sign}(b/E)$  for  $E^2 < |b|$  and  $\text{sign}(K_{-\theta}^\theta) = \text{sign}(E)$ ,  $\text{sign}(K_{+\theta}^\theta) = -\text{sign}(E)$  for  $E^2 > |b|$ .

#### 3.2 Proper time relations

By setting  $k = 1$  it follows from (6) the condition

$$N = u \geq +1, \quad (42)$$

i.e., on each side of the junction surface proper time must proceed faster (with respect to the time coordinate) than on the junction surface. To investigate the resulting constraints on the surface energy density we start by noting that

$$|w'(wK_{-\theta}^\theta) - a| - |\dot{w}L| \begin{cases} \geq 0 & \text{for } a \geq 0 \\ \leq 0 & \text{for } a \leq 0 \end{cases}, \quad (43)$$

which can be easily verified by squaring and substituting from (34). Substituting (38) the inequality (42) takes the form

$$\frac{(w'(wK_{-\theta}^\theta) - a) - \dot{w}L}{a} \geq 0.$$

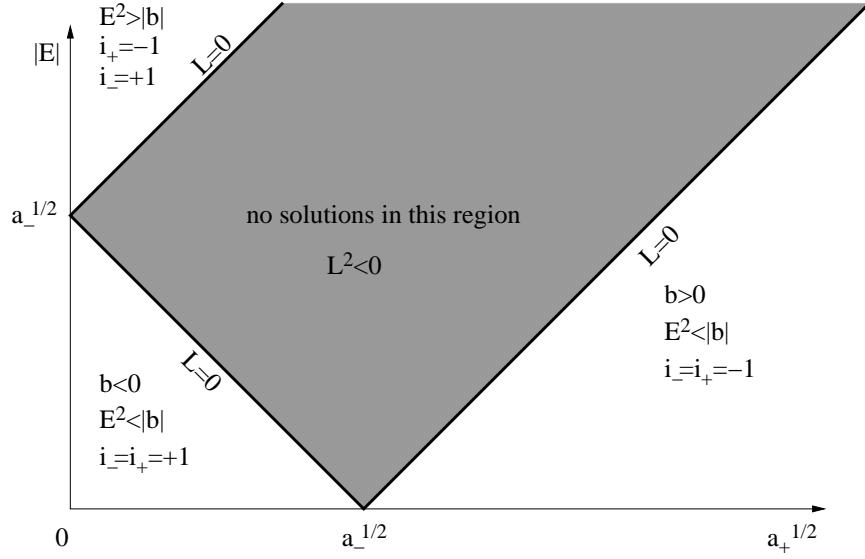


Figure 5: Region in the  $E - \sqrt{a_+}$ -plane where there is no solution for the junction surface motion for positive  $a_+$  and  $a_-$ . On the bold line we have  $E = |\sqrt{a_+} \pm \sqrt{a_-}|$  and hence  $L = 0$ . Each of the three different allowed regions is distinguished by the signs of the extrinsic curvature and the surface energy density  $i_{\pm} \stackrel{\text{def}}{=} \text{sign}(K_{\pm\theta}^{\theta}) \cdot \text{sign}(E)$ .

It follows from (43) that for  $a > 0$  we need

$$w'(wK^{\theta}_{\theta}) - a \geq 0,$$

while for  $a < 0$

$$\dot{w}L \geq 0. \quad (44)$$

Let us first consider the case  $a > 0$ . Using (35) the condition becomes

$$w' \frac{b + \sigma E^2}{-2E} - a \geq 0,$$

where  $\sigma = \pm 1$  corresponding to the outside (+) and inside (-) case. In the following let us use the convention that if  $a, w$  refer to the quantities on one side, then  $a_*, w_*$  refer to the quantities on the other side of the junction. By setting  $x \stackrel{\text{def}}{=} \text{sign}(b)E/\sqrt{|b|}$ ,  $\epsilon_{\pm} \stackrel{\text{def}}{=} \pm \text{sign}(b) = a - a_*$ , and

$$s_{\pm} \stackrel{\text{def}}{=} -\frac{a_{\pm}}{w'_{\pm}\sqrt{|b|}}$$

we bring the inequality in the form

$$\frac{1}{x} + \epsilon_{\pm} x \begin{cases} \leq 2s_{\pm} & \text{for } w'_{\pm} > 0 \\ \geq 2s_{\pm} & \text{for } w'_{\pm} < 0 \end{cases}. \quad (45)$$

The allowed ranges for  $x$  are illustrated in figure 6.

**The case of  $\epsilon > 0$**  Let us note that if  $\epsilon_+ > 0$  then  $\epsilon_- < 0$  and vice versa ( $\epsilon_* < 0$ ). The sign of the surface energy density is now determined by

$$\text{sign}(\rho_s) = -\text{sign}(b)\text{sign}(w'). \quad (46)$$

Furthermore, if  $|s| = |a/(w'\sqrt{|b|})| \leq 1$  then no restrictions are placed on  $|x|$  (but further restrictions could come from  $a_* > 0$ ). For  $|s| > 1$  the allowed range can be found by setting  $|x| = e^z$  and hence  $|1/x + x| = 2 \cosh(z)$ . Using  $\cosh^{-1}|s| = \ln(|s| + \sqrt{s^2 - 1})$  one obtains the ranges

$$0 < |x| \leq |s| - \sqrt{s^2 - 1} \quad \text{or} \quad |s| + \sqrt{s^2 - 1} \leq |x|.$$

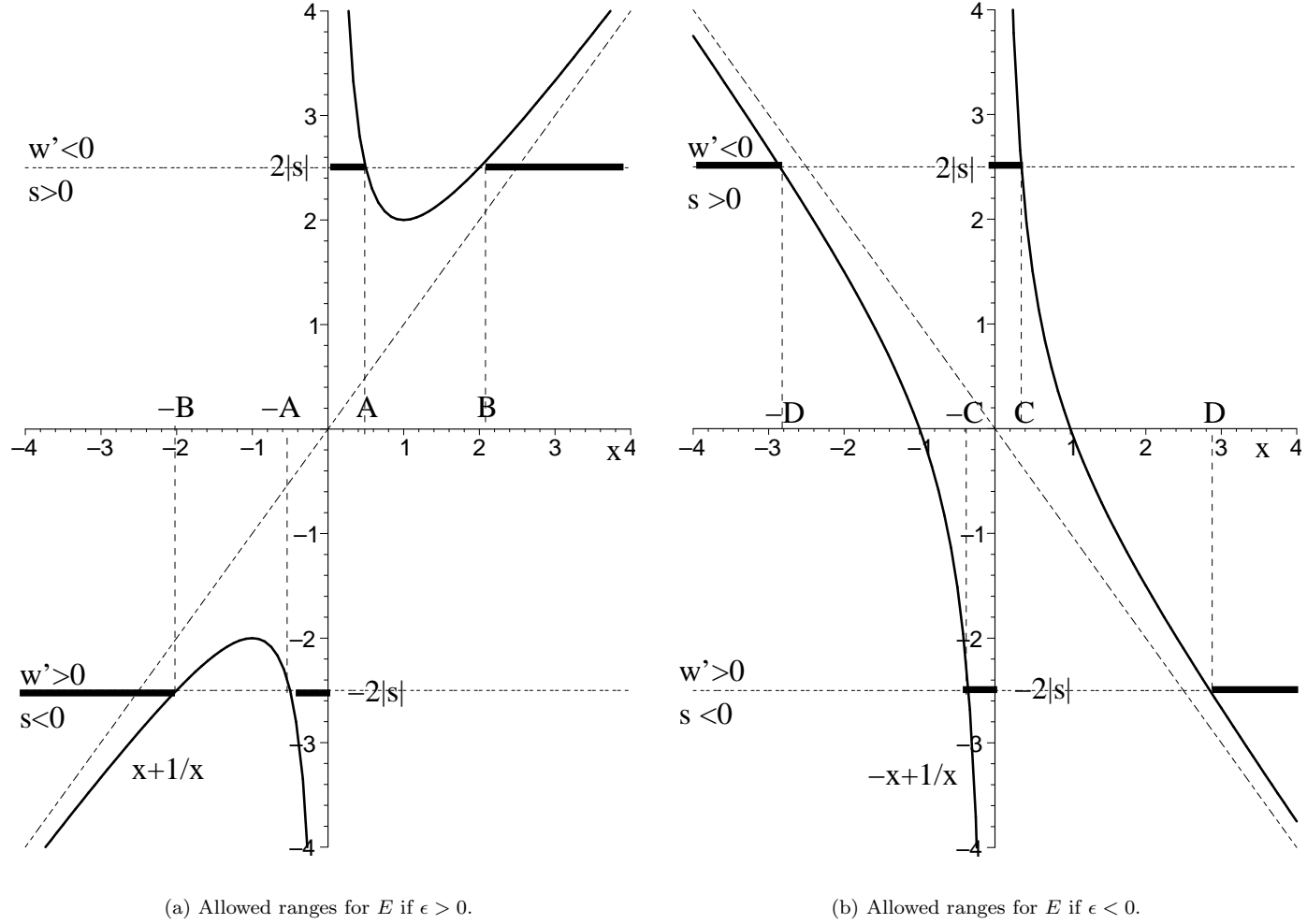


Figure 6: Visualization of the inequality (45) for  $\epsilon > 0$  (figure 6(a)) and  $\epsilon < 0$  (figure 6(b)). The lower and upper horizontal line correspond to  $w'_{\pm} > 0$  and  $w'_{\pm} < 0$ , respectively. Here  $s_{\pm} \stackrel{\text{def}}{=} -a_{\pm}/(w'_{\pm}\sqrt{|b|})$  are the terms on the right-hand side of (45). The allowed ranges are indicated by a bold line. The end-points are given by ( $A$  and  $B$  are only defined for  $|s| > 1$ )  $A = |s| - \sqrt{s^2 - 1}$ ,  $B = |s| + \sqrt{s^2 - 1}$ ,  $C = -|s| + \sqrt{s^2 + 1}$ ,  $D = |s| + \sqrt{s^2 + 1}$ .

**The case of  $\epsilon < 0$**  Similarly to the last case, if  $\epsilon < 0$  then  $\epsilon_* > 0$ . Hence each case will occur once at the junction. A similar procedure as above yields the restrictions

$$|s| - \sqrt{s^2 + 1} \leq \text{sign}(w')x < 0 \quad \text{or} \quad |s| + \sqrt{s^2 + 1} \leq \text{sign}(w')x.$$

**The case of  $a > 0$  on both sides** If  $a$  is positive on both sides then  $x$  can only take values which lay in the intersection of the allowed ranges on each side. The allowed intervals differ, depending on the signs of  $w'_+$  and  $w'_-$ . All possible cases are shown in table 1. We note that in every case the allowed values for  $E$  have the same sign.

As a particularly important case (for the matching of FLRW models) and an illustrative example we evaluate the restrictions on the surface energy density for  $a_+, a_- > 0$  and  $w'_+, w'_- > 0$ . In this case  $x$  has to be negative and hence

$$\text{sign}(\rho_s) = \text{sign}(E) = -\text{sign}(b).$$

If one assumes on physical grounds that  $\rho_s$  should be positive then no matching will be possible if  $b$  is positive.

**The case of  $a < 0$**  If  $a < 0$  on one side of the junction surface then (44) implies with

$$\text{sign}(L) = \text{sign}(\dot{w})$$

the sign for  $L$ , the coordinate time derivative of the surface radius, which was left undefined in (36). For the case that  $a_+$  and  $a_-$  are negative this condition must hold on both sides and hence a matching is only possible if

$$\text{sign}(\dot{w}_+) = \text{sign}(\dot{w}_-) \quad \text{for } a_+, a_- < 0. \quad (47)$$

## 4 The time-component of the Lanczos equation

So far we have only considered matching of the metric and of the angular components of the extrinsic curvature of the junction surface. The remaining matching condition comes from the time-component of the extrinsic curvature (22), which contains a second order time derivative of the junction coordinate radius, or equivalently a first-order time derivative of the lapse function.

Rewriting the time-component of the extrinsic curvature in terms of our variable  $u = N/k$  yields

$$-K^{\mu\nu}u_\mu u_\nu = \frac{j}{\sqrt{u^2 - 1}} \frac{du}{dt} + j\sqrt{u^2 - 1} \frac{\dot{l}}{l} + u \frac{N'}{N}, \quad (48)$$

where the factor  $N'/N$  is independent of the junction surface motion. Taking the coordinate time derivative of (35) and using (29) and (37) we obtain

$$\frac{j_\pm L}{\sqrt{u_\pm^2 - 1}} \frac{du_\pm}{dt} = -\frac{1}{2E} \frac{db}{dt} - \frac{dE}{dt} \frac{1}{E} w K_{\mp\theta}^\theta - z, \quad (49)$$

where (note that  $(d/dt)f(t, \alpha(t)R) = u\dot{f} + j\sqrt{u^2 - 1}f'$ )

$$z \stackrel{\text{def}}{=} u \frac{dw'}{dt} + j\sqrt{u^2 - 1} \frac{d\dot{w}}{dt} = ju\sqrt{u^2 - 1}\{w'' + \ddot{w}\} + u^2(w')^\bullet + (u^2 - 1)(\dot{w})'.$$

Differentiating (33) and using (27) with  $u^a|_a = 2L/w$  yields

$$\frac{dE}{dt} = -\kappa L \left( \frac{\rho_s}{2} + p_s \right) + \kappa \frac{w}{2} [T_{\mu\nu} u^\mu n^\nu],$$

which expresses the coordinate time derivative of  $E$ . Substituting for the first term in (48) allows us to evaluate the remaining junction condition  $[K^{\mu\nu}u_\mu u_\nu] = -\kappa(\rho_s/2 + p_s)$ . The terms containing the surface pressure and density cancel each other and we obtain

$$0 = \frac{\kappa}{2} w [T^{\mu\nu} u_\mu n_\nu] + [z] - L \left[ j\sqrt{u^2 - 1} \frac{\dot{l}}{l} \right] - L \left[ u \frac{N'}{N} \right]. \quad (50)$$

	$b > 0$ $\Rightarrow \epsilon_+ = +1, \epsilon_- = -1$	$b < 0$ $\Rightarrow \epsilon_+ = -1, \epsilon_- = +1$
$w'_+ > 0$ $w'_- > 0$	$\text{sign}(\rho_s) = -1$ $\sqrt{ b } \max(-A_+, -C_-) \leq E < 0$ for $ s_+  > 1$ $-\sqrt{ b }C_- \leq E < 0$ for $ s_+  \leq 1$	$\text{sign}(\rho_s) = +1$ $0 < E \leq \sqrt{ b } \min(A_-, C_+)$ for $ s_+  > 1$ $0 < E \leq \sqrt{ b }C_+$ for $ s_+  \leq 1$
$w'_+ > 0$ $w'_- < 0$	$\text{sign}(\rho_s) = -1$ $E \leq \sqrt{ b } \min(-B_+, -D_-)$ for $ s_+  > 1$ $E \leq -\sqrt{ b }D_-$ for $ s_+  \leq 1$	$\text{sign}(\rho_s) = -1$ $E \leq \sqrt{ b } \min(-B_-, -D_+)$ for $ s_-  > 1$ $E \leq -\sqrt{ b }D_+$ for $ s_-  \leq 1$
$w'_+ < 0$ $w'_- > 0$	$\text{sign}(\rho_s) = +1$ $\sqrt{ b } \max(B_+, D_-) \leq E$ for $ s_+  > 1$ $\sqrt{ b }D_- \leq E$ for $ s_+  \leq 1$	$\text{sign}(\rho_s) = +1$ $\sqrt{ b } \max(B_-, D_+) \leq E$ for $ s_-  > 1$ $\sqrt{ b }D_+ \leq E$ for $ s_-  \leq 1$
$w'_+ < 0$ $w'_- < 0$	$\text{sign}(\rho_s) = +1$ $0 < E \leq \sqrt{ b } \min(A_+, C_-)$ for $ s_+  > 1$ $0 < E \leq \sqrt{ b }C_-$ for $ s_+  \leq 1$	$\text{sign}(\rho_s) = -1$ $\sqrt{ b } \max(-A_-, -C_+) \leq E < 0$ for $ s_-  > 1$ $-\sqrt{ b }C_+ \leq E < 0$ for $ s_-  \leq 1$

Table 1: For  $a_+ > 0$  and  $a_- > 0$  this table shows the allowed region for  $E$  for all possible combinations of  $\text{sign}(w'_+)$  and  $\text{sign}(w'_-)$ . Here  $A_\pm = |s_\pm| - \sqrt{s_\pm^2 - 1} \leq 1$ ;  $B_\pm = |s_\pm| + \sqrt{s_\pm^2 - 1} \geq 1$ ;  $C_\pm = -|s_\pm| + \sqrt{s_\pm^2 + 1} \leq 1$ ;  $D_\pm = |s_\pm| + \sqrt{s_\pm^2 + 1} \geq 1$ . and  $s_\pm = -a_\pm / (w'_\pm \sqrt{|b|})$ .

The first term can be expressed in terms of the Einstein-tensor with respect to the original metric (1) as

$$\kappa T_{\mu\nu} u^\mu n^\nu = G_{\mu\nu} u^\mu n^\nu = ju\sqrt{u^2-1} \left( \frac{G_{tt}}{N^2} + \frac{G_{rr}}{l^2} \right) + (2u^2-1) \left( \frac{G_{tr}}{Nl} \right),$$

where the relevant components of the Einstein-tensor are given by

$$\begin{aligned} G_{tt} &= \frac{2N^2}{w} \left( -w'' + \dot{w} \frac{\dot{l}}{l} + \frac{1-a}{2w} \right) \\ G_{rr} &= \frac{2l^2}{w} \left( \ddot{w} - w' \frac{N'}{N} + \frac{1-a}{2w} \right) \\ G_{tr} &= \frac{2Nl}{w} \left( \dot{w} \frac{N'}{N} - (w')^\bullet \right), \end{aligned}$$

and  $L$  is given by (30). Substituting into (50) and using the relation

$$(\dot{w})' - (w')^\bullet = \frac{\dot{l}}{l} w' - \frac{N'}{N} \dot{w}$$

shows that (50) is an identity, satisfied *for all* spherically symmetric junctions between solutions of the Einstein-field equations if the geometric matching conditions ((4) and (5)) together with the angular component of the Lanczos equation (32) are satisfied. While it was well-known that for certain cases the time-component of the Lanczos equation is identically satisfied (e.g. [8, 11]), it seems to be a new result for the generic spherically symmetric case.

It was suggested that for the matching of FLRW models the time-component of the Lanczos equation determines the pressure [9]. In light of the above result this cannot be the case and one needs to supplement the model with an equation of state for the surface-matter.

## 5 Matching of FLRW sections

We want to turn our attention now to the special case of the matching of two distinct FLRW regions. Such junctions are encountered in cosmological models which approximate universes containing many FLRW domains (multidomain universes). The most prominent example is Linde's Chaotic Inflation scenario [3, 4].

Junctions of this type have been studied in [9, 13]. Our treatment will serve as an illustration for the introduced method and as a source for numerical examples. Here it is not our aim to investigate physical processes which could lead to the creation of a "bubble" and we refer the interested reader to the vast literature (see, e.g., [9, 14, 15, 16, 17]). Instead we want to focus on the generic geometrical and mathematical aspects.

### 5.1 FLRW models and their parametrization

The metric of FLRW models can be written in the form

$$ds^2 = -N^2(t)dt^2 + l^2(t)\{dr^2 + f^2(r)d\Omega^2\}, \quad (51)$$

where  $l(t)$  is the scale factor,  $N(t)$  the so-called lapse function,  $d\Omega$  the line-element on the two-dimensional unit-sphere, and

$$f(r) = \begin{cases} \sin(r) & \text{for closed models} \\ r & \text{for flat models} \\ \sinh(r) & \text{for open models} \end{cases}.$$

Note that the FLRW metric (51) has the same form as the general metric for spherical symmetric spaces (1), but with  $l' = 0$ ,  $N'/N = 0$  and  $\dot{f} = 0$ .

The evolution of FLRW models is described by the Friedmann equation - the dynamic part of the Einstein-Field equations -

$$\left( \frac{\dot{l}}{l} \right)^2 - \frac{\kappa\rho + \Lambda}{3} = -\frac{\zeta}{l^2}, \quad (52)$$



where  $\zeta = 0, +1, -1$  for flat, closed, and open models, respectively, and a dot indicates the derivative with respect to *proper* time  $t$ , i.e.,  $\dot{l} \stackrel{\text{def}}{=} \frac{1}{N} \frac{dl}{dt}$ .

The matter is described by an energy-momentum tensor of perfect fluid type. The unit tangent vectors to the fluid flow lines are given by

$$v^\mu = \frac{1}{N} \delta_t^\mu - \frac{\dot{\alpha} R}{\alpha} \delta_R^\mu,$$

where we used the coordinates introduced in subsection 2.1, and the energy-momentum tensor takes the form

$$T^{\mu\nu} = (\rho + p)v^\mu v^\nu + pg^{\mu\nu},$$

where  $\rho$  is the energy density and  $p$  the pressure. The matter evolution is then described by the energy-conservation equation

$$\dot{\rho} + (\rho + p)3H = 0,$$

where  $H \stackrel{\text{def}}{=} \dot{l}/l$  is the Hubble parameter.

We restrict ourself to models with a  $\gamma$ -law equation of state, i.e., models in which energy density  $\rho$  and pressure  $p$  are related by<sup>2</sup>

$$p = (\gamma - 1)\rho \quad \gamma \in (2/3, 2].$$

In this case  $\chi_\gamma \stackrel{\text{def}}{=} \frac{\kappa}{3} \rho l^{3\gamma}$  is a constant of motion proportional to the entropy per coordinate volume. This allows us to eliminate the energy density  $\rho$  from the Friedmann equation, so that the evolution of the scale factor  $l$  is described in terms of the constants of motion by

$$H^2 = \chi_\gamma l^{-3\gamma} + \frac{1}{3} \Lambda - \frac{\zeta}{l^2}. \quad (53)$$

Taking the proper-time derivative of this equation we recover the Raychaudhuri equation, which takes the form

$$\ddot{l} = \frac{2 - 3\gamma}{2} \chi_\gamma l^{-3\gamma+1} + \frac{\Lambda}{3} l \quad (54)$$

for  $\dot{l} \neq 0$ .

## 5.2 Modelling transition regions

Often the space-time is modelled by two almost-FLRW sections which are continuously joined through a transition region as illustrated in figure 7(a). Each FLRW section is characterized by its constants of motion.

The non-FLRW region which constitutes the transition region allows for the change of these constants from one side to the other.

Even under the assumption of spherical symmetry such models are of a rather complex nature — there are many possible choices for the geometry of the transition region, which should asymptotically approach the FLRW geometry on each side. Finding an exact solution to the Einstein field equation which models a particular transition region seems impossible.

Assuming that the thickness of the transition region is small compared to the length scale of the FLRW regions (Hubble length) one can model such a transition region by a junction surface as shown in figure 7(b). The surface-energy density then represents the ‘collective effect’ of the non-FLRW region.

## 5.3 Identification of models

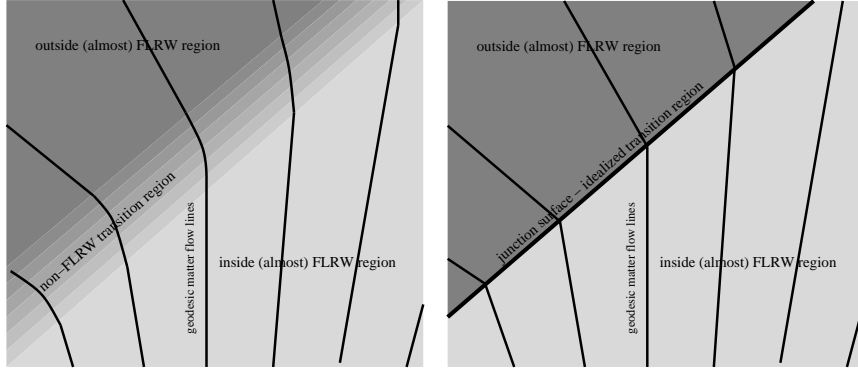
It will be of interest whether there are different models with the same evolution of the Hubble parameter  $H$ . For this purpose let us only consider models with a  $\gamma$ -law equation of state.

Let us first note that the Hubble parameter can be written as  $H = \frac{\dot{l}}{l} = (\ln(l))^\bullet$ . Hence models with the same evolution of  $H$  are models whose scale factors differ by a *constant* factor.

Let us assume we are given a solution to the Friedmann equation with  $\gamma = \gamma_-$ ,  $\chi = \chi_-$ ,  $\Lambda = \Lambda_-$ , and  $\zeta = \zeta_-$ . The question is now, whether there are constants  $\gamma_+$ ,  $\Lambda_+$ ,  $\chi_{\gamma_+}$  and  $\zeta_+$  such that  $l_+ = \lambda l_-$  is a solution

---

<sup>2</sup>The case  $\gamma = 0$  gives an effective cosmological constant. We can exclude this case here because the cosmological constant is included separately.



(a) Two (almost) FLRW regions are joined by a ‘thin’ non-FLRW region.

(b) The non-FLRW region is approximated as a surface.

Figure 7: Approximating a transition region by a junction surface simplifies the treatment.

for constant  $\lambda > 0$ . Both solutions would have the same Hubble parameter  $H \stackrel{\text{def}}{=} \frac{\dot{l}_+}{l_+} = \frac{\dot{l}_-}{l_-}$ . Substituting in each case from the Friedmann equation (53) gives

$$\chi_{\gamma_-} l_-^{-3\gamma_-} + \frac{1}{3} \Lambda_- - \frac{\zeta_-}{l_-^2} = \chi_{\gamma_+} l_-^{-3\gamma_+} \lambda^{-3\gamma_+} + \frac{1}{3} \Lambda_+ - \frac{\zeta_+}{l_-^2} \frac{1}{\lambda^2},$$

which has to be satisfied for all values of  $l_-$ . On both sides all terms contain different powers of  $l$  (note that  $-3\gamma \in (-2, 6]$ ). In order that both sides contain the same powers of  $l$  we need  $\gamma_- = \gamma_+$ . Comparing the coefficients gives then  $\lambda = 1, \zeta_+ = \zeta_-, \Lambda_+ = \Lambda_-$ , and  $\chi_{\gamma_+} = \chi_{\gamma_-}$ . Hence the solutions are identical.

We conclude that the evolution of the Hubble parameter  $H$  uniquely identifies a FLRW model with a  $\gamma$ -equation of state.

## 5.4 Matching without surface-layer

From the results of the previous section it is clear that it is impossible to join generic spherically symmetric sections along a timelike hypersurface without a surface-layer, i.e.,  $\rho_s = 0$ , except the metric satisfies some extraordinary conditions. In realistic models this could happen at most in singular situations and not along the whole trajectory of the junction hypersurface.

## 5.5 Comoving junction surface

Let us first investigate whether there could be a comoving junction surface, i.e., a junction surface at a fixed value of the comoving radial coordinate  $r$  inside and outside the bubble. In this case  $\dot{\alpha}_{\pm} = 0$  and from the geometric matching condition (specialized to the FLRW metric) (5) we find  $N_+ = 1$ . On the other hand (4) gives

$$l_+ = \underbrace{\frac{f_-(\alpha_-)}{f_+(\alpha_+)}}_{\text{const.}} l_-, \quad (55)$$

where the first factor is now time-independent. Given the result from the preceeding section we conclude that if the inside and outside of the bubble are evolving according to the Friedmann equation (52) with a  $\gamma$ -law equation of state then the inside and outside region must be identical in order to satisfy (55).

We note that this result follows alone from the geometric matching condition (5) – it does not depend on the presence of a surface layer.

## 5.6 Matching of FLRW regions with surface-layer

The FLRW metric (51) implies  $w = l(t)f(r)$  and by taking proper-time and radial derivatives we derive

$$\dot{w} = Hlf = Hw \quad \text{and} \quad w' = \frac{df}{dr}.$$

The component of the energy-momentum tensor which is needed to evaluate the surface-matter evolution according to (27) is easily found to be (for completeness we include  $k$ , which is set to unity)

$$[T^{\mu\nu}u_\mu n_\nu] = \left[ \frac{N^2 \dot{\alpha} l(\rho + p)}{k^2} \right].$$

We proceed now by expressing all quantities related to the metric and its derivatives ( $a, b, w', \dot{w}$  etc.) in terms of FLRW model quantities. With  $(df/dr)^2 = 1 - \zeta f^2$  we obtain the expressions

$$a = 1 - f^2(H^2 l^2 + \zeta) \stackrel{(52)}{=} 1 - \frac{\kappa\rho + \Lambda}{3} w^2 = 1 - w^2 H^2 \Omega.$$

$$b = a_+ - a_- = -\frac{w^2}{3}[\kappa\rho + \Lambda] = -w^2[H^2\Omega] = -w^2 \left[ \frac{\Omega}{l^2|\Omega - 1|} \right].$$

First we want to examine which kind of bubbles could exist if there can only be a positive surface-energy density on the junction surface, i.e.,  $E > 0$ . For reasonably small bubbles we have

$$a_+ > 0 \quad a_- > 0 \quad w' > 0.$$

We find from table 1 that in this case

$$\text{sign}(E) = -\text{sign}(b) = \text{sign}([\kappa\rho + \Lambda]),$$

and hence junctions are only possible if the inside FLRW region has a smaller total<sup>3</sup> energy density than the outside region. This is illustrated in figure 8(a). Figure 8(b) shows the allowed cases in the  $\Omega_- - \Omega_+$ -plane for equal scale-factors. The case  $\kappa\rho_+ + \Lambda_+ = \kappa\rho_- + \Lambda_-$  corresponds to the ‘no surface-layer’ case.

## 5.7 A particular example

To understand the behaviour of the junction surface it is instructive to consider a particularly simple example for which the evolution equations are known. One such example is the junction between a non-inflating closed geometry with radiation inside ( $\Lambda_- = 0, \zeta_- = +1$ ) and an inflating empty open geometry outside ( $\chi_+ = 0, \zeta_+ = -1$ ).

For these cases the Friedmann equation (53) is easily integrated and one finds the well-known solutions

$$l_-(\tau_-) = \sqrt{2\tau_- \chi_- - \tau_-^2} \quad l_+(\tau_+) = \sqrt{\frac{3}{\Lambda_+}} \sinh \left( \sqrt{\frac{\Lambda_+}{3}} \tau_+ \right), \quad (56)$$

where  $\tau_+$  and  $\tau_-$  are the proper times outside and inside, respectively. For the inside model the scale factor  $l_-$  grows until it reaches a maximum at  $\tau_- = \chi_-$ , and then declines until it reaches zero at  $\tau_- = 2\chi_-$ . On the contrary the outside model expands exponentially forever.

Since for each time  $t$  the proper time measured along the junction surface is always less or equal to the proper time in the inside and outside model ( $u_\pm \geq 1$ ) it is clear that such a boundary can only exist for a finite proper time measured along the junction — the (timelike) junction surface must be ‘terminated’ at some time.

There are four possible solutions. Firstly, it is possible that the junction surface exists forever (in terms of the proper time) in the outer region while the proper time along the junction surface is bounded. In our formalism this corresponds to a non-integrable divergence in the lapse function  $N_+ = u_+$  for the outer region.

Secondly, the junction surface can contract to a point such that the inner region is eliminated. This case is characterized by  $\alpha_+$ ,  $\alpha_-$  and  $w$  approaching zero at some finite time.

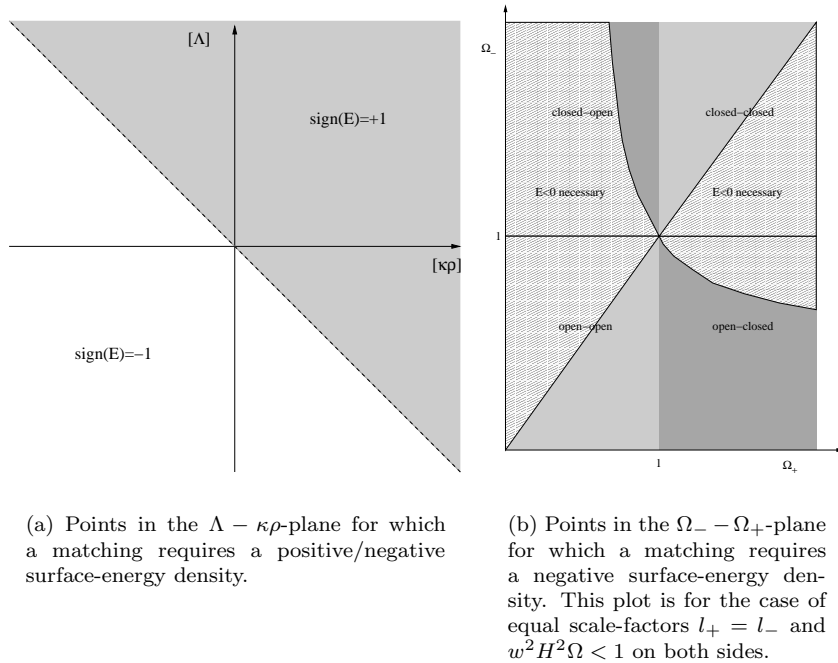


Figure 8: Only certain matchings are possible if there can only be a positive surface energy density.

Thirdly, the closed surface might detach from the open geometry — the birth of a child universe. In this case the radial coordinate for the closed geometry  $\alpha_-$  approaches  $\pi$ , while  $\alpha_+$  and  $w$  vanish (see figure 10).

As a last option the outside region might be eliminated. In the case of a closed outside geometry this is surely a possible solution, but in the cases of flat and open outside geometries this generally requires that the junction surface turns spacelike<sup>4</sup>.

In our formalism such a behaviour would yield a diverging, but integrable, lapse function. At the singularity we reach the speed of light and our formalism breaks down. Nevertheless, of the three options, to become super luminal, to continue at the speed of light, or to decelerate, the first one seems most convincing, also with view on the results of section 2.6.

Generally, one of these cases has to occur before we reach the singularity in the inside region as can be seen from the following argument. Let us assume that for physical reasons only positive surface energies are allowed. Since the outside geometry is open we have  $w'_+ > 0$ . As the closed inside geometry approaches the ‘big crunch’ singularity the energy density grows without bound. Hence  $b = w^2(\kappa\rho_- - \Lambda_+)$  has to become positive at some stage during the contraction phase. However, from table 1 one can see that there is no solution possible with  $w'_+ > 0$  and  $b > 0$  if  $a_+$  and  $a_-$  are positive. Let us note that when the inside region is contracting we have  $\dot{w}_- < 0$  and  $\dot{w}_+ > 0$ . Hence according to (47)  $a_+$  and  $a_-$  cannot be both negative. If  $a_+$  is positive (and  $a_-$  negative) then (46) implies that the surface energy density is negative, which is in contradiction with our assumption. If on the other hand  $a_+ < 0$  then this implies  $L > 0$  and hence the proper surface radius would increase. This just helps driving  $a_- = 1 - \kappa\rho_- w^2/3$  closer to zero, which eventually has to turn negative due to the diverging energy density. Again we reach a point where no solution is possible without negative surface energies.

Note that if one allows negative surface energies then the above argument shows that if the junction starts with a positive surface-energy density then at some point the junction must have a vanishing surface-energy density. For a generic situation this implies that at this point the junction moves with the speed of light.

Figure 14 shows the results of a numerical integration of this particular model. It appears as if the speed of light is reached within a finite time (integrable lapse functions) on both sides. This strongly suggests to us that the junction turned spacelike. Note that this happens even far before the inner closed region enters

<sup>3</sup>The cosmological constant represents the vacuum energy density.

<sup>4</sup>One might speculate that for a closed inside geometry there has to be a finite volume and hence the junction surface has to turn backwards in time and become timelike again.

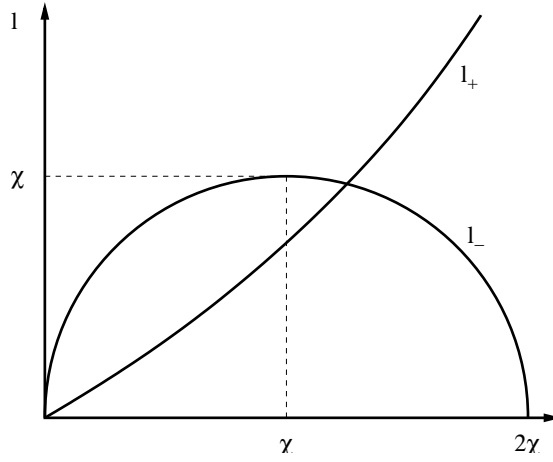


Figure 9: Evolution of the scale factor in a closed non-inflating FLRW model ( $l_-$ ) and in an empty open inflating model ( $l_+$ ).

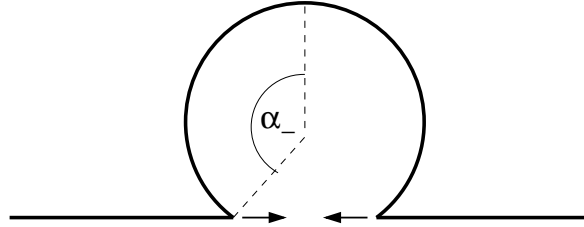


Figure 10: The closed inside geometry can detach from the open outside geometry. This happens when  $\alpha_- \rightarrow \pi$  within a finite time.

the contracting phase.

With this example we want to emphasize that there might be junctions which are possible initially, but which evolve to some singular point. As can be seen from the numerous examples in the next section this behaviour appears to be rather common.

## 6 Numerical Results

A computer program has been written to integrate the evolution equations for several FLRW junctions numerically. To achieve better accuracy around the singularities a variable step-width was used. All examples given here are for positive surface-energy densities. Cases with negative surface energy can easily be constructed by exchanging the inside and outside region. The graphs on the following pages illustrate the results and will be discussed one-by-one below.

- *Open inside, inflating closed geometry outside* Figure 11 shows such an example. After some time the surface radius starts to diverge (note the logarithmic scaling) while  $E = \kappa w \rho_s / 2$  does not approach zero (hence close to the divergence  $\rho_s \propto 1/w$ ). The proper times on both sides seem to be diverging, which is in agreement with the results from subsection 2.6. Note that the inner and outer regions have a rather unusual equation of state with  $\gamma_+ = 0.7$  and  $\gamma_- = 1.9$  — in this case it is really this choice of the equations of state which makes the energy-momentum tensor contribution  $[T_{\mu\nu} u^\mu n^\nu]$  positive for small values of  $E$  (see subsection 2.6).

Figure 12 shows the evolution of the same initial situation, but with different equations of state (dust on both sides). This seems to change the sign of the energy-momentum contribution  $[T_{\mu\nu} u^\mu n^\nu]$  for small values of  $E$ , which now approaches zero within a finite time. In fact, it can be verified that close to the singular point  $t_0$  we have as expected  $E \propto \sqrt[3]{t_0 - t}$ . As predicted in subsection 2.6 the lapse

functions appear to be integrable and the proper times do not diverge. The junction surface seems to reach the speed of light within a finite time.

Clearly, our formalism breaks down at this point. However, one could argue that after reaching the speed of light within a finite time, one should expect the junction to turn spacelike.

- *Closed inside, inflating open outside* Such a case with dust-equations of state on each side is illustrated in figure 13. Similarly to the last case  $E$  seems to reach zero within a finite coordinate and proper time.

Figure 14 shows a similar situation, but with a radiation equation of state for the inside region ( $\gamma_- = 4/3$ ). This is the example given in the previous subsection.

- *Flat inside with vacuum and inflating flat outside with radiation* This case is illustrated in figure 15. Note that here the coordinate radii and the proper speeds are plotted with respect to the proper time. Also in this case we encounter a non-integrable divergency in the lapse function. Note that in the outside region the bubble first grows and then shrinks for some time, before it enters a phase of indefinite expansion.

For the junction between two closed FLRW geometries figure 16 shows the evolution in the  $E - \sqrt{a_+/a_-}$  plane for different initial surface-energy densities.

## 7 Conclusion

We developed a formalism for the treatment of timelike junctions between spherically symmetric solutions of the Einstein-field equation, which is based on the Lanczos equation and the Israel junction conditions. We introduce new coordinates such that two conditions are satisfied: Firstly, all coordinates are continuous at the junction surface, and secondly, the junction surface becomes a surface of constant ‘radial’ coordinate. In this approach the actual movement of the junction surface is absorbed into the metric, of which the transverse components are discontinuous at the junction surface.

We evaluate the junction conditions and re-discover with (34) and (35) well-known relations between the extrinsic curvatures, the surface layer energy density, and the rate of change of the surface radius of the junction surface. It should be pointed out that these results follow without using the time-component of the Lanczos equation. As it was shown in subsection 4, for all spherically symmetric cases this remaining equation is in fact an identity. This was known for special cases, but it appears to be a new result in this general form.

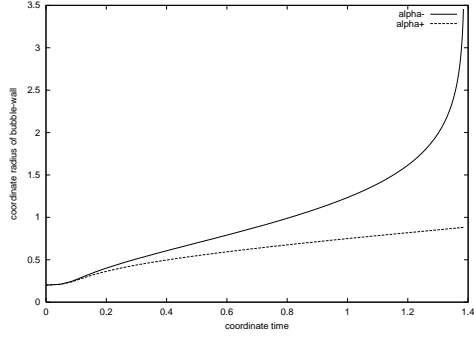
The behaviour for small values of  $E = \kappa w \rho_s / 2$  has been investigated. It was shown that for certain cases  $E$  is driven to zero within a finite coordinate and proper time. At such a point our formalism breaks down. Nevertheless, we want to speculate here that in such cases the junction really turns spacelike. This can be seen as an inadequacy of the thin wall formulation in such situations — a causal propagation of a discontinuity should not exceed the speed of light. We suggest that in such cases the spatial extent of the transition region is not negligible.

The developed formalism gives us two sources for constraints on possible junctions. Firstly the time derivative of the surface radius is given by the quadratic equation (36). Demanding that real solutions to this equation must exist directly restricts the possible values of the surface energy density for a particular junction (see figure 5). Secondly, in our approach physical solutions must have a lapse function which is greater than or equal to unity. The resulting restrictions depend on the metric components on each side of the junction — they either determine the sign of the derivative of the proper surface radius, or they restrict the possible surface-energy densities (see figure 6). For the latter case the allowed ranges for  $E = \kappa w \rho_s / 2$  have been given explicitly.

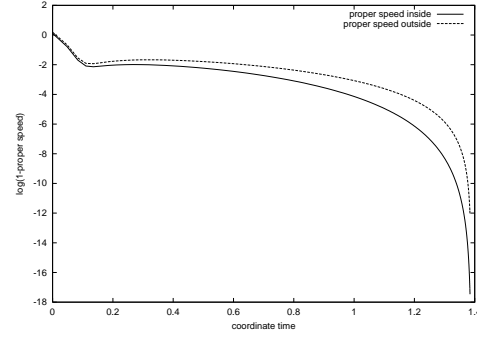
For the special case of junctions between FLRW models with  $\gamma$ -equation of state it was shown that alone on geometrical grounds there can be no comoving junction surface — whether with or without surface layer.

A particularly interesting model, the junction between an empty, open, inflating FLRW region outside and a radiation dominated closed FLRW model inside, has been investigated in more detail. The inside region re-collapses after some finite proper time and hence the junction surface has to be terminated. Besides a disappearance or a detachment of the closed inner region we suggest that the junction can turn spacelike — an effective disappearance of the outer region.

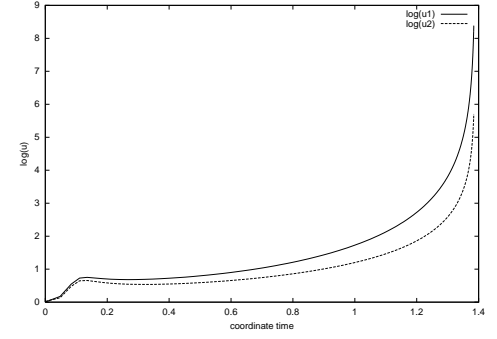
This and other examples have been integrated numerically. It was observed that many models seem to reach the speed of light within a finite *proper* time, in accordance with the predictions from section 2.6.



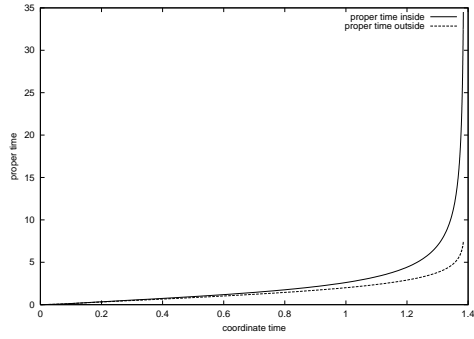
(a) Coordinate radius of the junction surface on each side



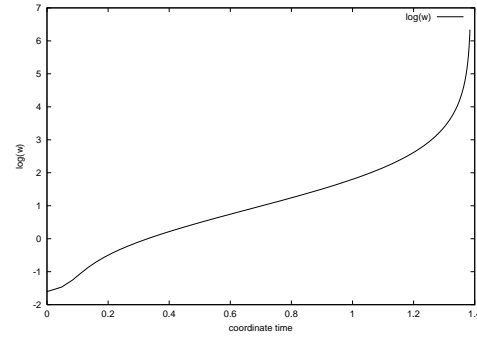
(b) Proper speed of the junction surface on each side.



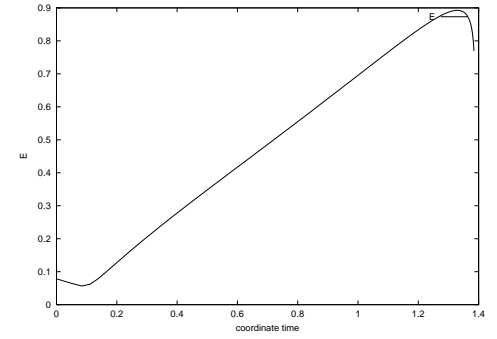
(c) Lapse function  $N = u$  on each side



(d) Proper times on both sides

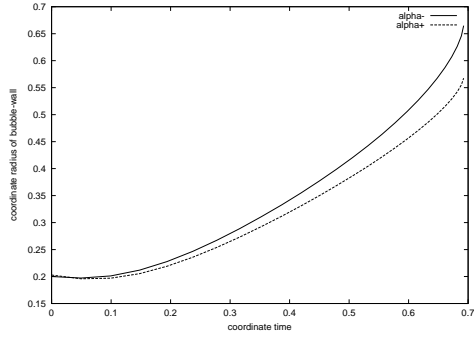


(e) Surface radius ( $w$ ).

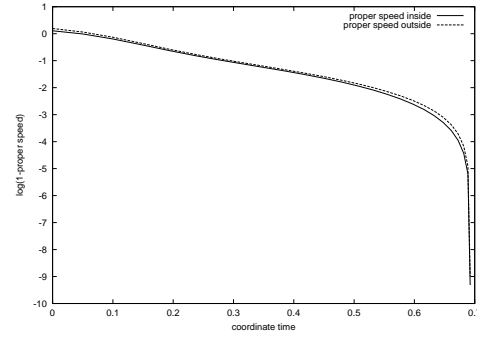


(f)  $E$ , which is related to the surface-matter energy density  $\rho_s$  by  $E = \kappa w \rho_s / 2$ .

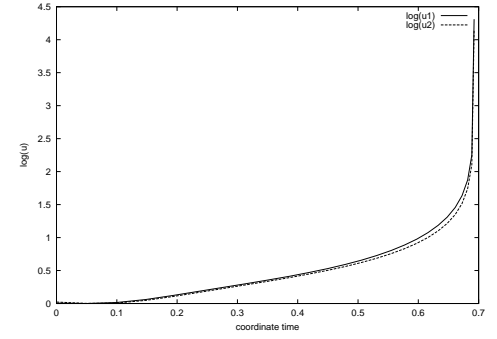
Figure 11: Evolution of a junction between an open (inside) and an inflating closed (outside) geometry. (Parameters:  $\gamma_s = 1, \zeta_+ = +1, \zeta_- = -1, \chi_+ = 5, \chi_- = 2, \gamma_+ = 0.7, \gamma_- = 1.9, \Lambda_+ = 2, \Lambda_- = 0$ ; Initial values:  $\rho_s = 0.031, \alpha_+ = 0.20272, \alpha_- = 0.2, l_+ = 1, l_- = 1, \rho_+ = 0.597, \rho_- = 0.239$ .) Note that here  $u$  and  $w$  are plotted logarithmically.



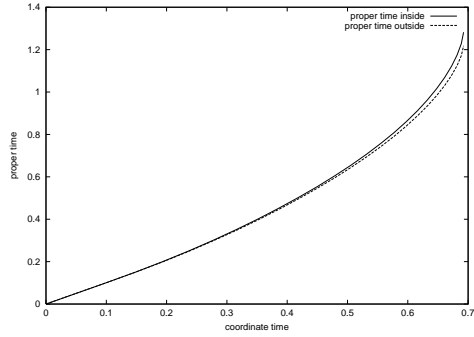
(a) Coordinate radius of the junction surface on each side



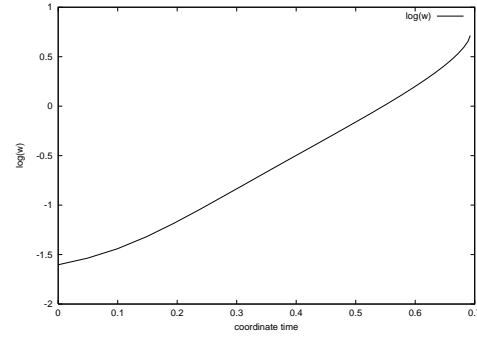
(b) Proper speed of the junction surface on each side.



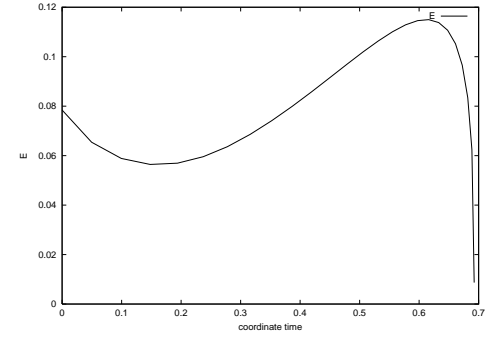
(c) Lapse function  $N = u$  on each side



(d) Proper times on both sides



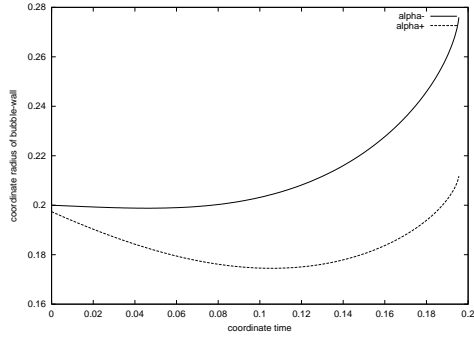
(e) Surface radius ( $w$ ).



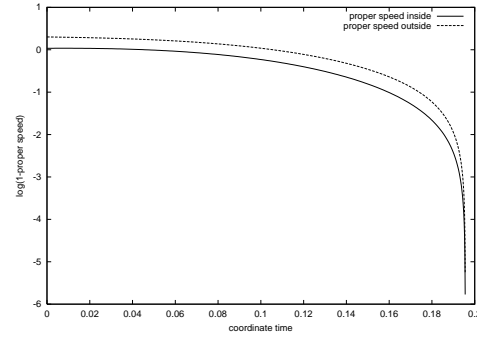
(f)  $E$ , which is related to the surface-matter energy density  $\rho_s$  by  $E = \kappa w \rho_s / 2$ .

Figure 12: Evolution of a junction between an open (inside) and an inflating closed (outside) geometry. The lapse functions are integrable and the speed of light is reached within a finite time. (Parameters:  $\gamma_s = 1, \zeta_+ = +1, \zeta_- = -1, \chi_+ = 5, \chi_- = 2, \gamma_+ = 1, \gamma_- = 1, \Lambda_+ = 2, \Lambda_- = 0$ ; Initial values:  $\rho_s = 0.031, \alpha_+ = 0.20272, \alpha_- = 0.2, l_+ = 1, l_- = 1, \rho_+ = 0.597, \rho_- = 0.239$ .) Note that here  $u$  and  $w$  are plotted logarithmically.

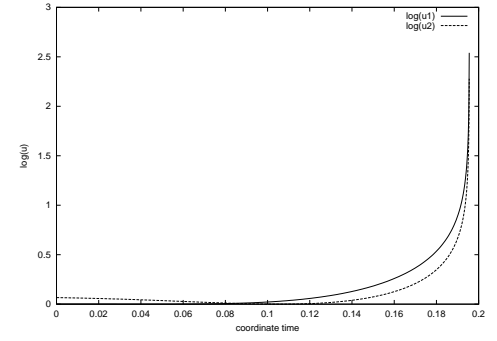




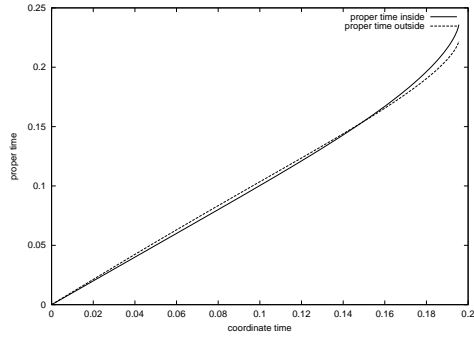
(a) Coordinate radius of the junction surface on each side



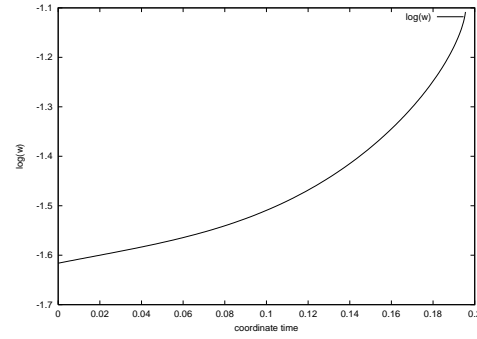
(b) Proper speed of the junction surface on each side.



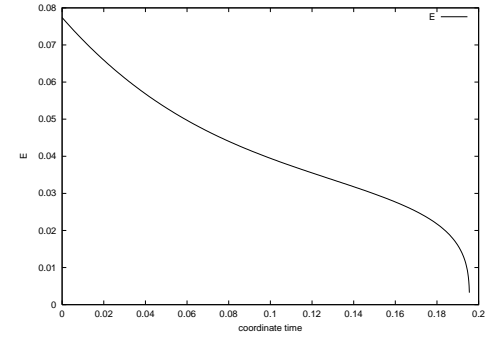
(c) Lapse function  $N = u$  on each side



(d) Proper times on both sides

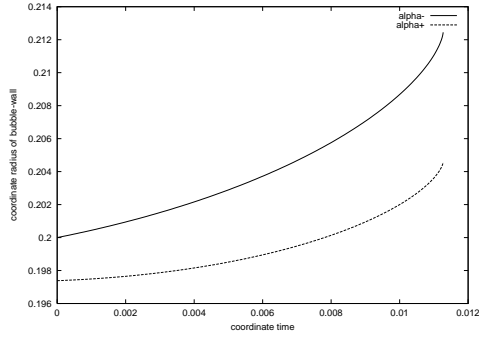


(e) Surface radius ( $w$ ).

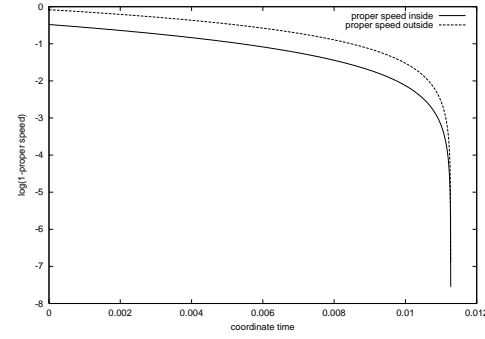


(f)  $E$ , which is related to the surface-matter energy density  $\rho_s$  by  $E = \kappa w \rho_s / 2$ .

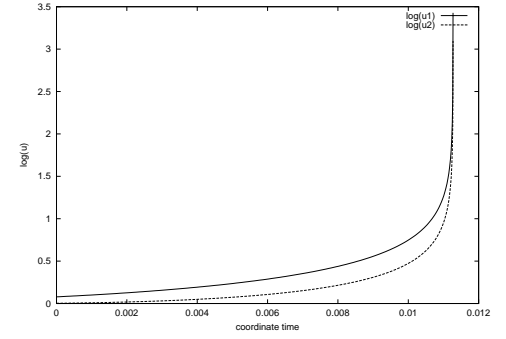
Figure 13: Evolution of a junction between a closed (inside) and an inflating open (outside) geometry. (Parameters:  $\gamma_s = 1, \zeta_+ = -1, \zeta_- = +1, \chi_+ = 5, \chi_- = 2, \gamma_+ = 1, \gamma_- = 1, \Lambda_+ = 2, \Lambda_- = 0$ ; Initial values:  $\rho_s = 0.031, \alpha_+ = 0.19739, \alpha_- = 0.2, l_+ = 1, l_- = 1, \rho_+ = 0.597, \rho_- = 0.239$ .) Note that here  $u$  and  $w$  are plotted logarithmically.



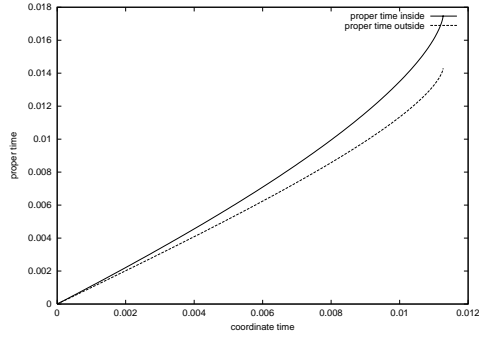
(a) Coordinate radius of the junction surface on each side



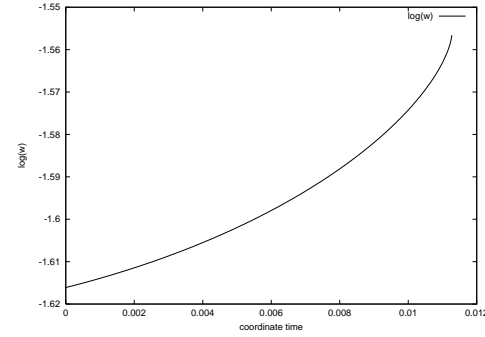
(b) Proper speed of the junction surface on each side.



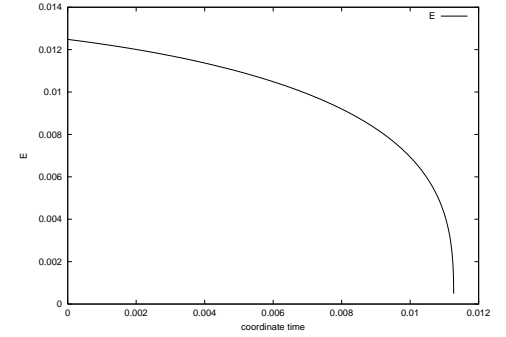
(c) Lapse function  $N = u$  on each side



(d) Proper times on both sides

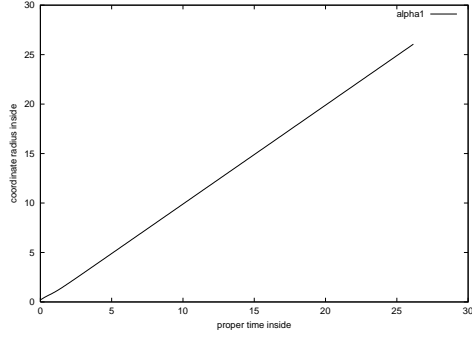


(e) Surface radius ( $w$ ).

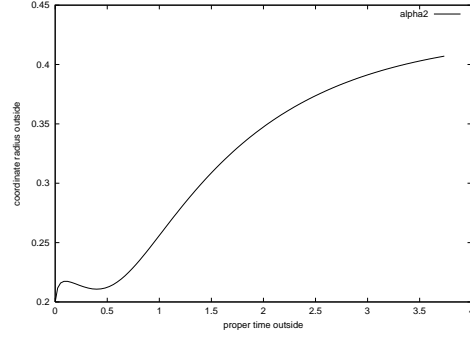


(f)  $E$ , which is related to the surface-matter energy density  $\rho_s$  by  $E = \kappa w \rho_s / 2$ .

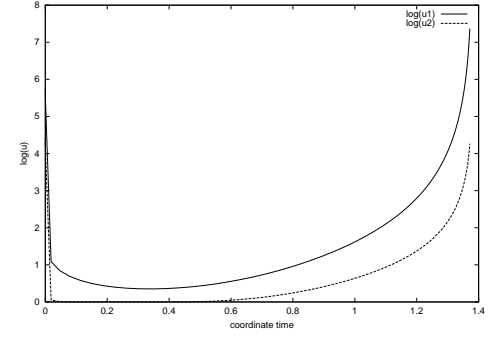
Figure 14: Evolution of a junction between a closed (inside) and an inflating open (outside) geometry. The inside has a radiation equation of state, while the outside is an inflating dust model. (Parameters:  $\gamma_s = 1, \zeta_+ = -1, \zeta_- = +1, \chi_+ = 0, \chi_- = 1, \gamma_+ = 1, \gamma_- = 4/3, \Lambda_+ = 5, \Lambda_- = 0$ ; Initial values:  $\rho_s = 0.005, \alpha_+ = 0.19739, \alpha_- = 0.2, l_+ = 1, l_- = 1, \rho_+ = 0, \rho_- = 0.119$ .) Note that here  $u$  and  $w$  are plotted logarithmically.



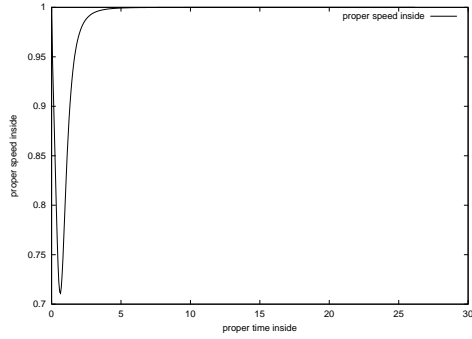
(a) Coordinate radius of the junction surface inside.



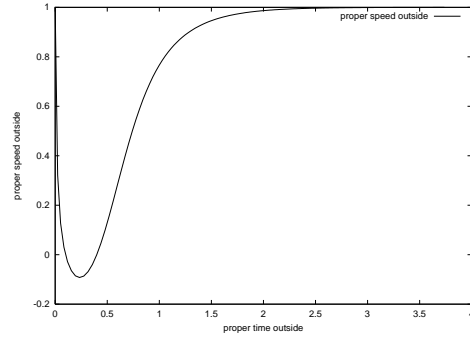
(b) Coordinate radius of the junction surface outside.



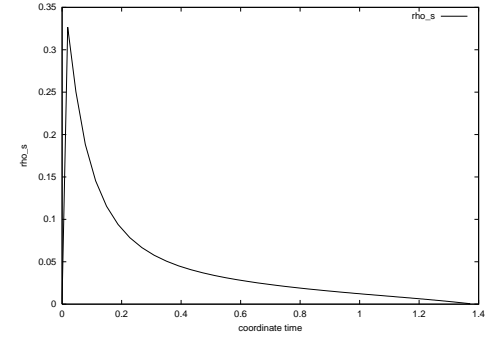
(c) Lapse function  $N = u$  on each side



(d) Proper speed inside.



(e) Proper speed outside.



(f) Surface-matter energy density  $\rho_s$ .

Figure 15: Evolution of a junction between two flat geometries. The outside has a radiation equation of state and is inflating, while the inside is vacuum model. (Parameters:  $\gamma_s = 1, \zeta_+ = +0, \zeta_- = +0, \chi_+ = 200, \chi_- = 0, \gamma_+ = 1.33, \gamma_- = 1, \Lambda_+ = 2, \Lambda_- = 0$ ; Initial values:  $\rho_s = 0.005, \alpha_+ = 0.2, \alpha_- = 0.2, l_+ = 1, l_- = 1, \rho_+ = 23.9, \rho_- = 0$ .) Note that here  $u$  is plotted logarithmically.

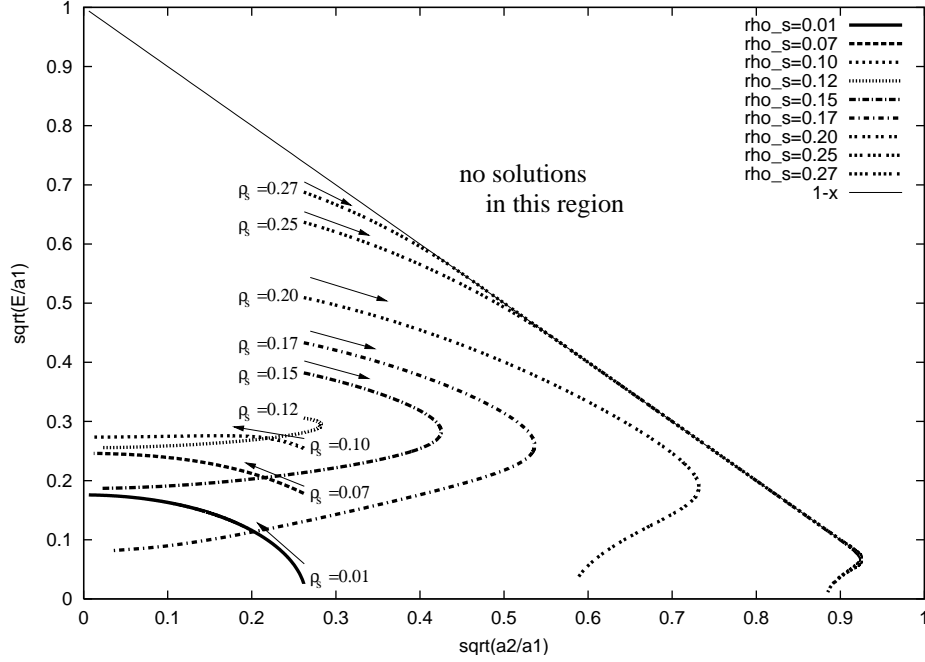


Figure 16: Evolution of junctions between two closed geometries in the  $|E|/\sqrt{a_-} - \sqrt{a_+/a_-}$  plane. The different trajectories correspond to different initial-values of the surface-energy density  $\rho_s$ . All other initial parameters are constant.

Since a spacelike junction violates causality, we suggest that a breakdown in the thin-wall approximation must have occurred.

Our results show that the thin-wall treatment of timelike junctions (without the presence of scalar fields) is on a *mathematical* sound level. Nevertheless, in many cases the junction surface reaches a singular point within a finite proper time. We believe that in these cases the thin-wall is not a *physically* acceptable approximation.

## References

## References

- [1] Spergel D N *et al* 2003 *Astrophys. J.* (Preprint astro-ph/0302209)
- [2] Guth A H 1981 *Phys. Rev. D* **23** 347
- [3] Linde A D 1983 *Phys. Lett. B* **129** 177
- [4] Linde A D 1990 *Particle Physics and Inflationary Cosmology* (Chur:Harwood Academic Publishers)
- [5] Lanczos C 1922 *Phys. Zeits.* **23** 539; and 1924 *Ann. der Phys.* **74** 518
- [6] Dautcourt R 1964 *Math. Nachr.* **27** 277
- [7] Israel W 1966 *Nuovo Cimento B* **44** 4349
- [8] Blau S K, Guendelman E I and Guth A H 1987 *Phys. Rev. D* **35** 1747
- [9] Berezin V A, Kuzmin V A and Tkachev I I 1987 *Phys. Rev. D* **36** 2919
- [10] Lake K 1987 in *Vth Brazilian School of Cosmology and Gravitation*, Ed. Novello, World Scientific, Singapore, pp1-82

- [11] Hájíček P and Biřák J 1997 *Phys. Rev. D* **56** (*Preprint* gr-qc/9706022)
- [12] Misner C W, Thorne K S and Wheeler J A 1973 *Gravitation*, W. H. Freeman and Company, San Francisco
- [13] Sakai N and Maeda K 1994 *Phys. Rev. D* **50** 5425-5428 (*Preprint* gr-qc/9311024)
- [14] Coleman S and De Luccia F 1980 *Phys. Rev. D* **21** 3305
- [15] Jensen L G and Steinhardt P J 1984 *Nucl. Phys. B* **237** 176-188
- [16] Lyth D H and Stewart E D 1994 *Preprint* hep-ph/9408324
- [17] Amendola L *et al* 1996 *Preprint* astro-ph/9610038